University of Strathclyde

Department of Physics

Nonlinear Frequency Conversion of Optically Pumped Vertical External Cavity Surface Emitting Lasers

Stefanie Renaud Keatings

in fulfilment of the requirements for the degree of MPhil

2011

This thesis is the result of the author's original research. It has been composed by the author and has not been previously submitted for examination which has led to the award of a degree.

S Keatings
March 2011

Abstract

We will present an overview of a home-built frequency doubled VECSEL and analysis of its optical pump profile. The system comprised an AlGaAs VECSEL emitting at 980 nm which was then frequency doubled via a single pass through the nonlinear crystal potassium niobate ($KNbO_3$). The resultant 490 nm source represents a reliable, cost and energy efficient alternative to typical argon lasers traditionally used in confocal laser scanning microscopy (CLSM). We will present CLSM images of various biological samples taken using this source, which is particularly well suited to exciting dyes such as Alexa 488, FITC and Kaede, as well as the increasingly-prevalent green fluorescent protein.

We will then demonstrate a further system which offers higher fundamental power incident at the crystal and therefore more efficient frequency doubling of the 980nm VECSEL light. This is achieved by placing the $KNbO_3$ doubling crystal in an external cavity in which the fundamental VECSEL power is enhanced (resonant frequency doubling). In this set-up the roundtrip lengths of the VECSEL cavity and the resonant ring cavity are exactly matched, so that all the longitudinal modes of the oscillating multimode VECSEL light are resonant inside the enhancement cavity. This system offers new and improved potential for biophotonics applications and opens up possibilities for other nonlinear frequency conversion processes within the external resonator configuration. The sum frequency generation of the resonant VECSEL light and a 1047nm Nd YLF source to provide high power pulsed blue light at 504nm and this system's potential for applications will also be discussed.

Acknowledgements

I would first and foremost like to my supervisor Erling Riis. Thank you so much for all your support, guidance, encouragement and friendship. I am honoured to have worked with you and thank you for giving me the opportunity to do so.

Thank you also to my second supervisor Gail McConnell. I have learned so much from you and because of your encouragement I have gained and grew in confidence. You are not just a great supervisor but also a true friend.

I would also like to thank Dr Thorsten Ackemann and Dr Aidan Arnold for their supervisory support in some of the experiments. I am thankful for your time and guidance in and outwith the lab.

Thank you to Dr Paul Griffin, Dr Kyle Gardner, Dr Elric Esposito and Dr Wei Zhang for helping me to find my feet in the lab and providing great assistance in the (many) times that things went a bit wrong.

Thanks to the amazing guys and girls in the Photonics group and Centre for Biophotonics. Alessio, Aline, Alison, Chris, Greg, Ian, John, Kenneth, Mateuz, Matthieu & Neal. It has been a pleasure working with you all and I wish you all the very best for your future careers.

Thanks also to Bob Wylie and Euan Maclagan for all their technical assistance and support.

And finally thank you to my wonderful family Mum, Dad, Suzi and John. You have all been hugely supportive and understanding. Thank you Mum for the lifts to and from the lab every day, I will miss them very much when I'm all alone on the train. Thank you, John, for sticking by me through tough times and hard decisions and for our happy life together. I am blessed to have such an amazing family and fiancé.. Thanks for being so great!

Contents

Chapter 4 Confocal Laser Scanning Microscopy using a frequency doubled VECSEL

Chapter 5 Resonant Second Harmonic Generation

Chapter 6 Sum Frequency Generation

List of Figures

Chapter 1 Vertical external cavity surface-emitting lasers

Introduction

Vertical External Cavity Surface Emitting Lasers (VECSELs) are a relatively new type of semiconductor laser with their first report by Jiang in 1991 [1], Their design is taken from the vertical cavity surface emitting laser (VCSEL) with the removal of the top distributed Bragg Reflector (DBR) to incorporate an external mirror to complete the cavity, introducing the useful concept of the external cavity. The architecture of such lasers provides control of the lasing modes and allows additional optical elements to be employed within the external resonator cavity. In addition the VECSEL also has the advantage of being able to be optically pumped.

Unlike traditional semiconductor lasers, VECSELs inherently emit a TEM_{00} mode (circular, near, diffraction-limited beam) [2] which is ideal for high-resolution imaging applications and due to the flexible semiconductor structure of the gain medium associated to the external cavity, it is possible to tailor the emitting wavelength.

VECSELs are usually designed to emit in the infrared region but the output converted via various nonlinear frequency conversion techniques to provide useful, visible wavelength beams which will be the subject of the work in this thesis.

VECSELs are becoming increasingly recognised and acknowledged within the laser community and their areas for potential applications are being explored.
VECSELs have proved successful in the near-infrared with impressive power scaling [3], sub-picosecond modelocking [4], single frequency operation [5] and frequency doubling to selected wavelengths in the visible [6], particularly the blue wavelength region [7].
Tuneable blue frequency doubled VECSELS are ideal for applications in atom optics and biomedicine [8].

This chapter provides a brief outline of the basic configuration and operating principles of a VECSEL and describes the physical aspects of the source used in this work.

Design of Optically Pumped VECSELs

The basic cavity configuration of an optically pumped VECSEL is shown in Figure 1.

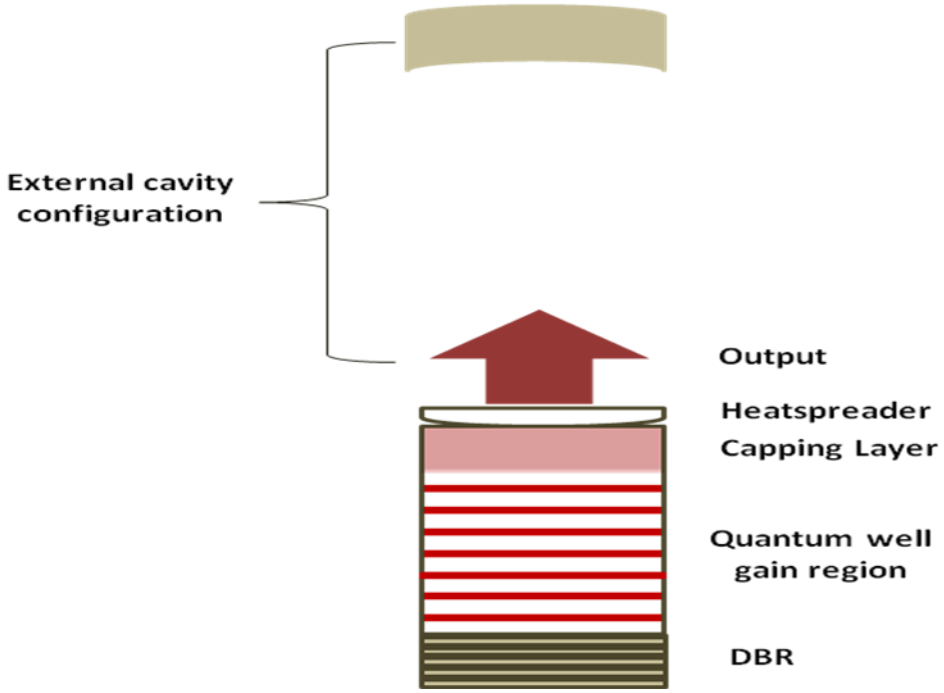

Figure 1 Basic configuration of a VECSEL

The design of the VECSEL is critical to its efficiency. The main areas to consider are the distributed Bragg reflector (DBR), the quantum well gain region, the capping layer thermal management, and the external resonator. Each of these will be described in greater detail in the following sections.

Distributed Bragg Reflector

As VECSELs typically have low effective gain they require mirrors with >99.9% reflectivity at the laser wavelength. Distributed Bragg reflectors (DBRs) are mirrors capable of such high performance. Constructed of multiple quarter wavelength thick layers of alternating material of low and high refractive index, DBRs satisfy the Bragg condition at the design wavelength.

Reflections at each interface add up constructively to give an enhanced overall reflectivity as illustrated in Figure 2.

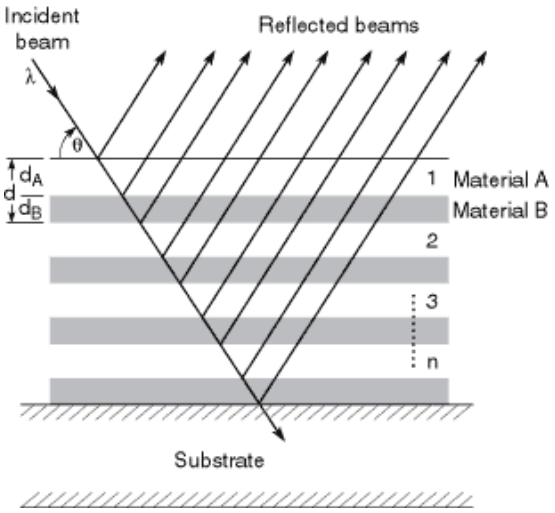

Figure 2 Distributed Bragg Reflector

The greater the refractive index difference, the greater the reflectivity, therefore for a high quality DBR, two lattice- matched semiconductor materials with high index contrast are required.

The VECSEL structure used in the following experiments employs a DBR made of 30 quarter-wave pairs of AlAs and GaAs layers with refractive indices n=3.2 and n=2.86 respectively.

Quantum Well Gain Region

The active region is grown on top of the DBR and is composed of multiple quantum wells (QWs) separated by barriers. The construction of the wells and barriers and the emission bandgap dictates the pump absorption and emission wavelengths. The pump light is absorbed in the barrier regions between the QWs and the generated carriers diffuse into the QWs from which they are then de-excited emitting photons at the desired emission wavelength, determined by the bandgap energy of the QW material. Designing the structure for the desired emission wavelength is known as bandgap engineering.

Multiple quantum wells are used to encourage a situation where the overall gain exceeds the losses in the material and hence lasing will occur. However if there are too many, all of the pump light will be absorbed in the regions between the QWs at the front of the structure and those at the back will serve only to act as losses, thus increasing the lasing threshold. An optimum number of quantum wells can be determined, which balances a low laser threshold with sufficient gain in which to exceed the cavity losses.

A gain region of 12, 8nm thick $In_{0.6}GaAs$ QWs separated by $Al_{0.06}GaAs$ barrier regions with a GaAsP strain compensating layer on either side is used in the following experiments. The structure materials have been chosen at the design stage in order that when the source is optically pumped by light at wavelength 808nm, the emission wavelength is 980nm. This material had previously been used for investigation of single frequency VECSELs [9].

Resonant Periodic Gain

Resonant period gain (RPG) is a technique incorporated into the design and growth of surface emitting lasers in an attempt to overcome the current limitations of these laser designs, particularly high thresholds and low efficiencies. These problems are mainly attributed to the extremely short gain length, lack of carrier and optical

confinement and generation of competing amplified spontaneous emission (ASE) in the transverse direction.

First employed in a VECSEL structure by Raja et al in 1988 [10], RPG enhances the gain through optimisation of the overlap between the gain medium and the optical field of a selected lasing mode by positioning the quantum wells at the antinodes of the standing wave optical field set up inside the material. In doing so the active regions occur only where required, and as the electric field is strongest at these points maximum gain can be extracted from the quantum wells. Raja reported the technique's successes as a reduction of the laser threshold and an increase in overall efficiency [11].

To satisfy the RPG condition the quantum wells are spaced at one half wavelength intervals within the active region and separated by passive barriers as illustrated in Figure 3. This structure forces the antinodes of the standing wave to coincide with the gain elements.

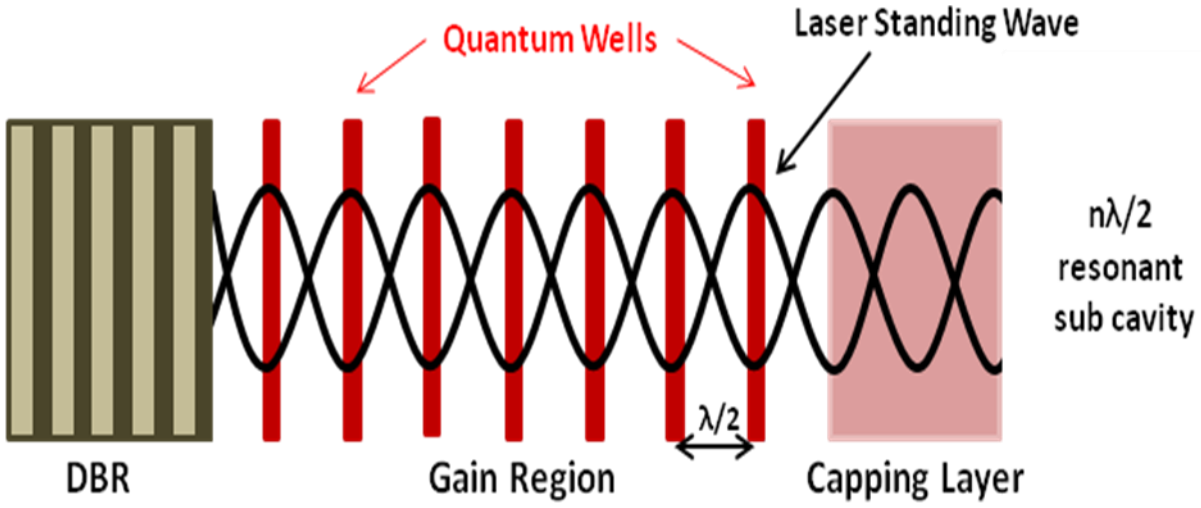

Figure 3 Resonant RPG structure

The length of the RPG gain region is mλ/2 where λ is the RPG wavelength and m is a positive integer. If the next layer, the capping layer's thickness is deliberately designed to be of thickness nλ/2 with n also a positive integer, then as well as the

main gain cavity, which extends from the DBR to the bottom surface of the capping layer, an additional sub cavity is formed between the DBR and the top surface of the capping layer which is resonant with the RPG wavelength and the structure is referred to as a resonant RPG structure.

Anti-resonant RPG VECSEL structures can be produced by designing the capping layer thickness to be nλ/2+λ/4 so that the sub cavity is anti-resonant with the RPG wavelength as shown in Figure 4.

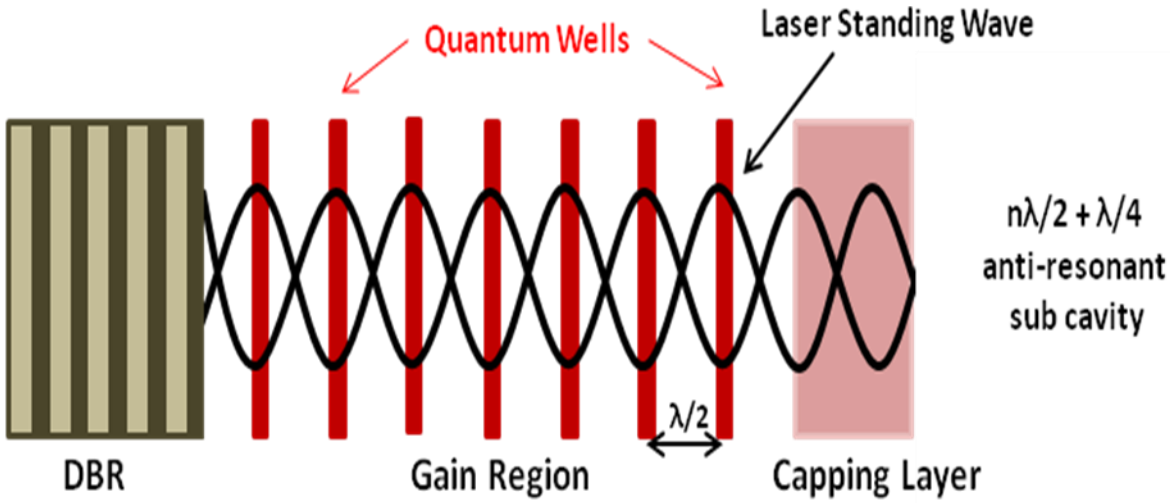

Figure 4 Anti-resonant RPG Structure

These anti-resonant structures have lower gain extraction than resonant structures however they have the compensating benefit of minimising the temperature sensitivity required for effective gain. In addition, without the spectral filtering effects induced in the resonant sub cavity, anti-resonant structures provide a larger gain bandwidth and therefore possess the ability of wavelength tunability.

As this work focuses on development of tuneable frequency conversion sources, an anti-resonant RPG designed VECSEL gain structure was used.

The Capping Layer

The role of the capping layer is to prevent carrier diffusion from the quantum well active region and to reduce oxidation of the microstructures by providing a barrier against oxygen in the atmosphere which can decay the structure over time.

It is a semiconductor material layer with a higher energy bandgap than that of the gain region material

The semiconductor materials chosen for the capping layer in this work are $Al_{0.3}GaAs$ and $In_{0.48}GaP$.

Thermal Management of VECSELs

One of the most significant factors limiting high-power CW operation in VECSELs is the build up of excess heat in the active region generated by optical pumping.

Unwanted thermal effects within the VECSEL system cause the output power to peak and then fall off dramatically with increasing pump power. This 'thermal rollover' effect can be attributed to 2 main effects.

Firstly, as the temperature in the gain region rises, free carriers confined in the quantum wells can be thermally re-excited and escape back up into the barrier regions. This decreases the population inversion and therefore the effective gain is reduced.

In addition, heating within the structure can misalign the RPG wavelength from the photoluminescence peak wavelength since both of these are shifted by different rates with increasing temperature. As a result, VECSELs will only operate efficiently at low temperatures where the two wavelengths coincide since beyond this the resonant features are no longer aligned.

To limit these effects, and delay the arrival of thermal rollover, pump-generated heat has to be efficiently extracted from the gain region.

Various methods of addressing the thermal management of VECSELs exist; including thermoelectric cooling [12] and thinning of [13], or complete removal, of the semiconductor substrate [14].

An alternative option which requires no post growth etching, pre-processing or alterations to the structure design, is the bonding of an optically transparent, high thermal conductivity single crystal onto the emitting surface of the structure which acts as a thermal channel extracting heat from the front surface of the VECSEL. This technique allows removal of the thermal excess much closer to the source of the heating than any of those mentioned above. The technique of using a crystalline heatspreader as a means of dissipating the pump induced heat generated in the VECSEL gain region was first reported by Alford et al in 2002 [15]. This group reported the first instance of high continuous wave output power from a VECSEL made possible by the use of a sapphire window optically contacted to the intracavity semiconductor surface for heat removal.

To date, this technique has been successfully demonstrated using a variety of crystalline materials as heatspreaders; including sapphire [16], silicon carbide [17] and diamond [18].

Comparing the thermal conductivity of these materials as well as that of the GaAs substrate it is clear that diamond is an ideal choice for heatsinking.

Material	Thermal Conductivity (W/cmK)
GaAs	0.46
Sapphire	0.4
SiC	5
Diamond	20
Ag	4.2

Table 1 Thermal conductivities of various materials

Diamond has the attractive properties of being the highest reported thermal conductivity of any solid [19], non-birefringent and optically transparent at

wavelengths from UV to far infrared and although traditionally fairly expensive it is now becoming available at moderate cost.

The use of diamond heatspreaders have increased the power scalability of the VECSEL with current output powers of several Watts achievable [20] and has widely increased the range of applications for which these devices can be used.

Although diamond proves to be a very effective heatspreader material, it has one major disadvantage in that it can act as an intracavity etalon, introducing additional surface reflections which can change the spectral output of the laser, narrowing the bandwidth and introducing unwanted spikes within it. This effect can be removed by using a wedged piece of diamond material rather than plane parallel.

In this work a 300μm thick anti-reflection (AR) coated single crystal wedged diamond heat spreader was contacted to the VECSEL wafer using the method of liquid capillary bonding first reported by Liau [21]. This method offered minimum thermal resistance and negligible optical losses with good contact and adherence to the semiconductor wafer. In order to achieve this type of bonding a tiny amount of distilled water was inserted between the extremely clean surfaces of the wafer and the crystal diamond piece and a reasonable pressure was applied until the water had fully evaporated. At this point, a capillary force bonds the two surfaces together by van de Waals interatomic attractions.

The External Laser Resonator

The VECSEL gain chip operates as an optically pumped end mirror in a linear 3-mirror folded cavity which is completed with external optical elements.

A schematic of the external cavity configuration is shown in Figure 5.

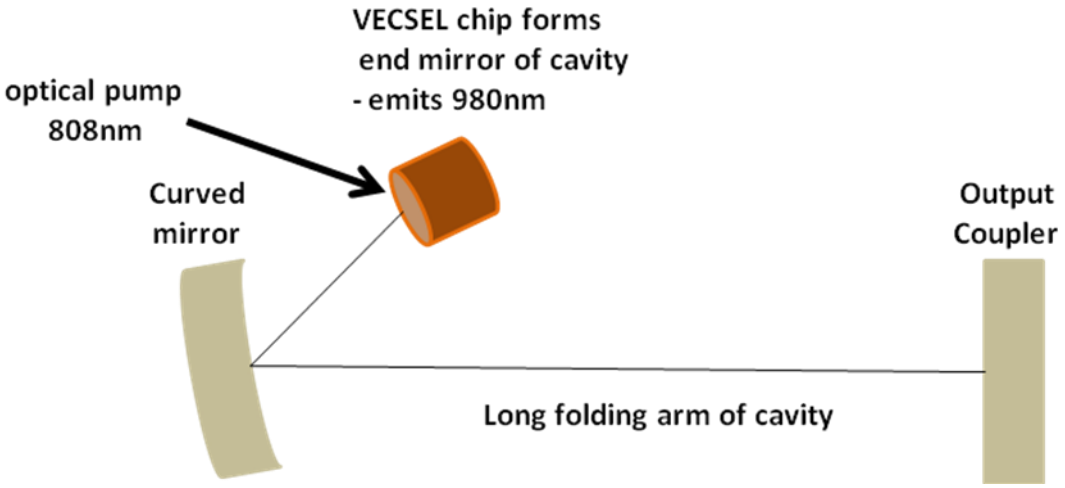

Figure 5 External Resonator Configuration

This work utilises a 3-mirror cavity instead of a simple 2-mirror cavity for the reason that 2-mirror cavities are inherently difficult to design construct and align. The 2-mirror cavity is extremely sensitive to critical alignment and often results in major instabilities and poor beam quality, making the source uncontrollable and unreliable.

The 3-mirror external resonator is designed to give a stable, good quality beam output and a desired cavity mode size to match the pump beam diameter.

The specific external cavity geometry for the VECSEL used in this work will be discussed in greater detail in Chapter 3.

Conclusion

This chapter has presented a brief introduction and outline of the basic configuration of VECSELs and has presented details of the VECSEL chip used throughout this work.

References

[1] Jiang W.B., Friberg S.R., Iwamura H., Yamamoto Y., High powers and sub picosecond pulses from an external cavity surface emitting InGaAs/InP multiple quantum well laser, Appl Phys Lett, **58**(8), 1991, 807

[2] Tropper A.C., Hoogland S., Extended cavity surface-emitting lasers, Progress in Quantum Electronics **30**(1), 2006, 1

[3] Chilla J.L., Butterworth S.D., Zeitschel A, Charles J.P., Caprara A.L., Reed M.K., Spinelli L, High power optically pumped semiconductor lasers, Solid State Lasers XIII: Technology and Devices, R Scheps and H J Hoffman, eds., Proc. SPIE **5332**, 2004, 143

[4] Garnache A., Hoogland S., Tropper A.C., Sagnes I, Saint-Girons G, Roberts J.S., Sub-500fs soliton-like pulse in a passively mode-locked broadband surface-emitting laser with 100mW average power, Appl. Phys. Lett, **80**, 2002, 3892

[5] Abram R.H., Gardner K.S., Riis E, Ferguson A.I., Narrow linewidth operation of a tunable optically pumped semiconductor laser, Optics Express, **12**(22), 2004, 5434

[6] Holm M.A., Ferguson A.I., Burns D, Dawson, Single-frequency second-harmonic generation in a vertical external cavity semiconductor laser, Conference on Lasers and Electro-optics (CLEO 2000) TOPS **39**, 2000, 440

[7] Raymond T.D., Alford W.J. Crawford M.H., Allerman A.A., Intracavity frequency doubling of a diode pumped external cavity surface emitting semiconductor laser, Opt Lett, **24**, 1999, 1127

[8] Risk W.A., Gosnell T.R., Nurmikko A.V., Compact Blue-Green Lasers, Cambridge University Press, 2003

[9] Single Frequency Vertical External Cavity Surface Emitting Lasers, K., S., Gardner, PHD Thesis, University of Strathclyde, 2007

[10] Raja M.Y.A., Brueck S.R.J., Osinski M., Schaus C.F., McInerney J.G., Brennan T.M., Hammons B.E., Novel wavelength-resonant optoelectronic structure and its application to surface-emitting semiconductor lasers, Electron. Lett. **24**, 18, 1988 1140

[11] Raja M.Y.A., Brueck S.R.J., Osinski M., Schaus C.F., McInerney J.G., Brennan T.M., Hammons B.E., Resonant periodic gain surface-emitting semiconductor lasers**,** IEEE Journ of Quant Elec, **25**, 6, 1989, 1500

[12] Holm M.A., Burns D., Cusumano P., Ferguson A.I., Dawson M.D., High-power diode pumped AlGaAs surface-emitting laser**,** Applied Optics, **38**, 27, 1999, 5781

[13] Hoogland S., Dhanjal S., Tropper A.C., Roberts J.S., Haring R., Paschotta R., Morier-Genoud F., Keller U., Passively mode-locked diode-pumped surface emitting semiconductor laser, IEEE Photonics Technol Lett, **12**, 9, 2000, 1135

[14] Haring R., Paschotta R., Aschwanden A., Gini E., Morier-Genoud F., Keller U., High-power passively mode-locked semiconductor lasers, IEEE Journ of Quant Elec, **38**, 9, 2002, 1268

[15] Alford W.J., Raymond T.D., Allerman A.A., High power and good beam quality at 980nm from a vertical external cavity surface-emitting laser, Journ of Opt Soc Am B, **19**, 4, 2002, 663

[16] Hastie J.E., Hopkins J.M., Calvez S., Jeon C.W., Burns D., Abram R., Riis E., Ferguson A.I., Dawson M.D., 0.5W single transverse-mode operation of an 850nm diode-pumped surface-emitting semiconductor laser, IEEE Photonics Technol Lett, **15**, 7, 2003, 894

[17] Bewley W.W., Felix C.L., Vurgaftman I., Stokes D., Aifer E.H., Olafsen L.J., Meyer J.R., Yang M.J., Lee H., Thermal characterization of diamond pressure bond heat sinking for optically pumped mid-infrared lasers, IEEE Journ Quant Elec, **35**, 11, 1999, 1597

[18] Wei L.H., Kuo P.K., Thomas R.l., Anthony T.R., Banholzer W.F., Thermal-conductivity of isotopically modified single-crystal diamond, Phys Rev Lett, **8**, 2-5, 1999, 909

[19] Fan L., Fallahi M., Hader J., Zakharian A.r., Moloney J.V., Murray J.T., Bedford R., Stoltz W., Koch S.W., Multichip vertical external cavity surface emitting laser: a coherent power scaling scheme, Optics Lett, **31**, 24, 2006

[20] Liau Z.L., Semiconductor wafet bonding via liquid capillarity, Appl Phys Lett, **77**, 5, 2000, 651

Chapter 2 Nonlinear Optics

Introduction

Since the advent of the laser in 1960 [1], laser scientists have endeavoured to create laser sources which operate over the entire wavelength spectrum. However, at present the range of optical pump sources and laser gain media available is limited mainly to those emitting in the infrared wavelength region. Sources that operate in other wavelength regions are sought for important emerging applications such as optical data storage [2], colour visual display technologies [3] spectroscopic applications [4] and biophotonics [5], with many of these requiring sources specific to the visible blue region which is the main focus of the work in this thesis.

It was the first frequency conversion experiment by Franken et al in 1961 [6] that introduced the concept of nonlinear optics and the subsequent developments in this field have led to a whole range of previously unobtainable wavelengths being accessed.

This chapter introduces the basic principles of nonlinear optics and describes in detail two nonlinear processes which are the focus of this work; second harmonic generation and sum frequency generation. The important conditions for optimised frequency conversion are also discussed.

Basic Principles of Nonlinear Optics

In order to understand the mechanism by which a beam(s) of light passed through a nonlinear crystal generates a beam of different frequency to that of the incoming beam(s), the following model is presented which although basic, captures the essential idea behind nonlinear frequency conversion [7].

A nonlinear crystal is made up of atoms which comprise of a positively charged centre (nucleus) surrounded by a cloud of negative charge (electrons orbiting the nucleus). In an equilibrium situation, with no beams incident on the crystal, the centres of positive and negative charge coincide as shown in Figure 6 (a) and there is no net polarisation present in the material.

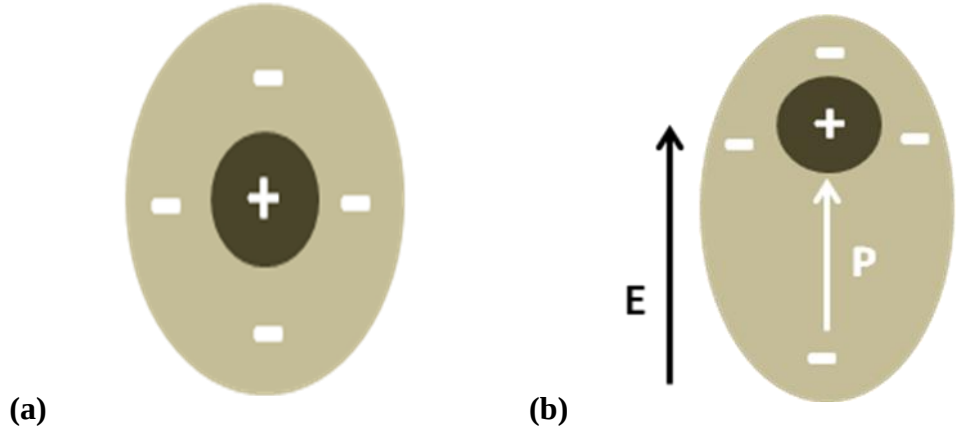

Figure 6 Atomic response to an electric field (a) equilibrium position, no electric field present (b) distortion of electron cloud due to the presence of an electric field [7]

However if a sinusoidal light wave, with frequency ω_1, is passed through the nonlinear medium, the time-varying electric field of the wave will exert a time-varying force on the electron cloud which causes a periodic spatial distortion of the positive and negative charge centres, as shown in Figure 6(b), resulting in the creation of an oscillating polarisation inside the material.

From classical electrodynamics we can recall that an accelerating charge radiates an electromagnetic wave, therefore if the relationship inside the material between the applied electric field and the generated polarization is linear, as shown in Figure 7 (a), the generated polarization will be sinusoidal at frequency ω_1 and the material will radiate its own electric field at frequency ω_1. This generated field interferes

with the original field passing through the material and the associated phase shift is due to the refractive index of the material [8].

If the relationship between the electric field and the induced polarisation in the material is not linear (as is the case for a nonlinear crystalline material) then the polarisation response to a sinusoidal field will be a distorted sinusoid, as shown in Figure 7(b). This distortion results in the presence of components at other frequencies in the polarisation response (such as $\pm 2\omega_1$ and $\omega_1 \pm \omega_2$ for a case of two input beams).

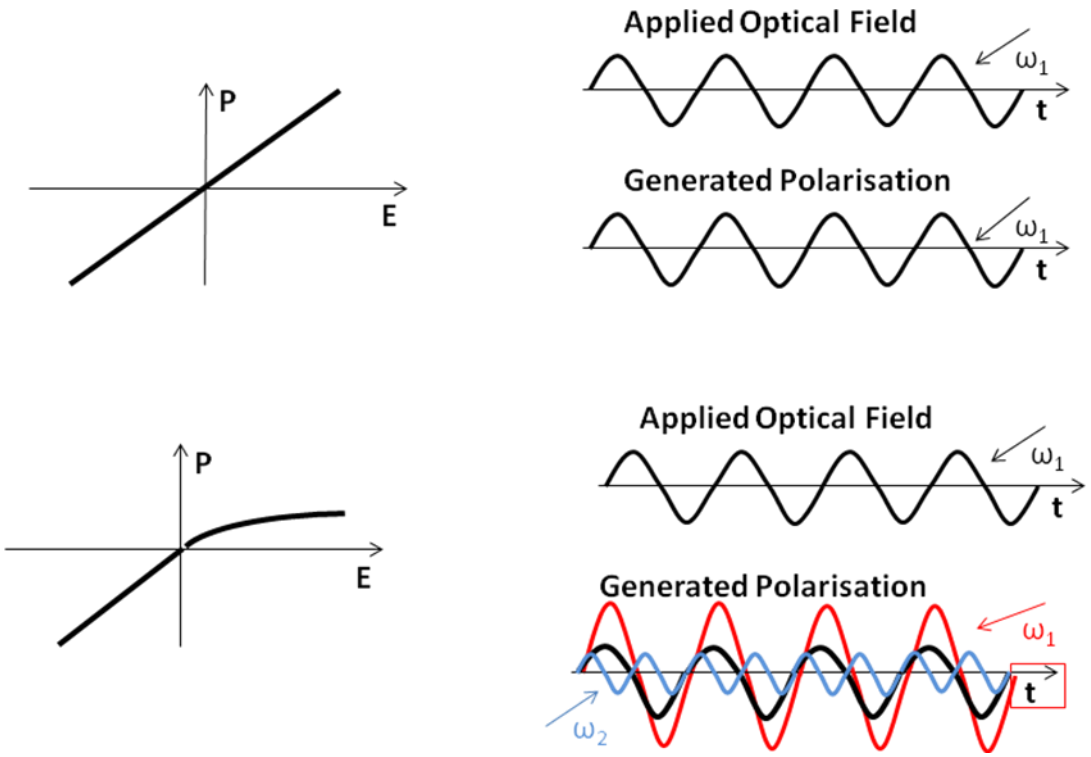

Figure 7 Relationship between the applied electric field and the generated polarisation (a) Linear (b) Non-linear

Described in mathematical terms, when a nonlinear crystalline medium is subjected to a large electric field the material has a nonlinear response and the polarisation, P, can be written as an expansion in powers of the applied electric field, E,

$$P = \varepsilon(\chi^{(1)} + \chi^{(2)}E + \chi^{(3)}E^2 + ...)E \qquad (1)$$

where ε is the permittivity of the medium and $\chi^{(n)}$ is the n^{th} order non-linear susceptibility.

The first term in this expansion gives rise to first-order linear phenomena such as index of refraction. The second order term gives rise to the nonlinear effects in which we are interested for the work in this thesis, namely second harmonic generation and sum-frequency mixing.

Second Harmonic Generation

Second harmonic generation (SHG), or frequency doubling, is a non-linear optical effect that occurs in birefingent nonlinear crystals which lack inversion symmetry. SHG is a response of crystals which exhibit the $\chi^{(2)}$ nonlinearity and in this process the response of an input wave of fundamental frequency ω_1 is to generate another wave at twice the optical frequency of the fundamental, $2\omega_1$ as shown in Figure 8.

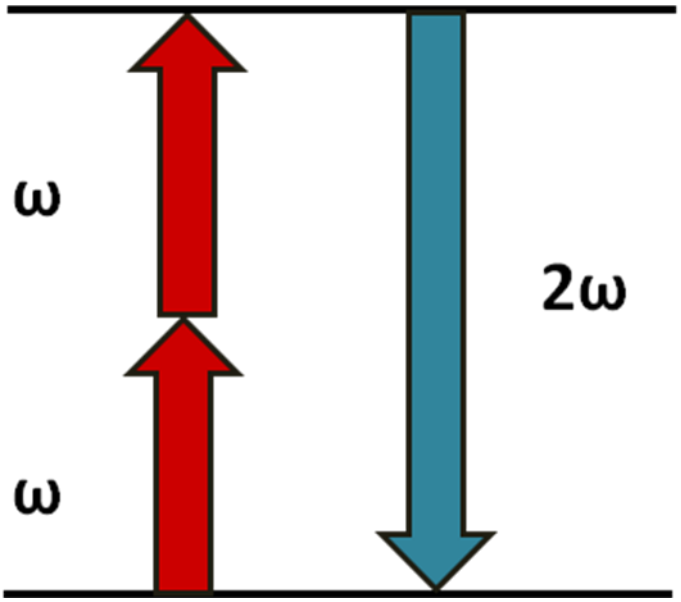

Figure 8 Energy-level diagram showing 2-photon absorption followed by single photon emission

From the theory of SHG first presented by Boyd and Kleinman [9], the expected intensity of the generated SHG beam $I_{2w}(l)$ for a fundamental input intensity I_w is calculated according to the equation

$$I_{2w}(l) = \frac{2\pi^2 d_{eff}^2}{\lambda_w^2 n_{2w} n_w^2 \varepsilon_0 c} l^2 I_w^2 sinc^2\left(\frac{\Delta k l}{2}\right) \quad (2)$$

where l is the crystal length, n_w and n_{2w} is the refractive index seen by the fundamental and SHG beam, λ_w is the wavelength of the fundamental, d_{eff} is the nonlinear coefficient which is a constant dependent on the electronic structure of the nonlinear crystal and $\Delta k = k_3 - 2k_1$ is the phase mismatch between the beams, where k_3 and k_1 are the propagation constants of the SHG and fundamental.

We can see from this equation, that the SHG intensity has a quadratic dependence on the fundamental intensity, the length of the nonlinear crystal and the nonlinear coefficient of the material. It is therefore desirable to choose experimental conditions (eg material type, crystal size and fundamental input) for which each of these factors are fully optimised.

The above equation assumes a monochromatic fundamental plane wave input. However if the source is multi-longitudinal with the input spectrum consisting of N closely spaced modes with uncorrelated phases, then the second harmonic power is enhanced by a factor 2-1/N. Hence as the number of modes N becomes large, the output second-harmonic power can become a factor of 2 larger than the case using a single frequency source. This effect was first observed by Ashkin in 1963 [10]

Phase Matching

From the above equation we can see that the efficiency of the frequency conversion process is optimised when the phase mismatch between the fundamental and the generated beam is zero, as also illustrated in Figure 9.

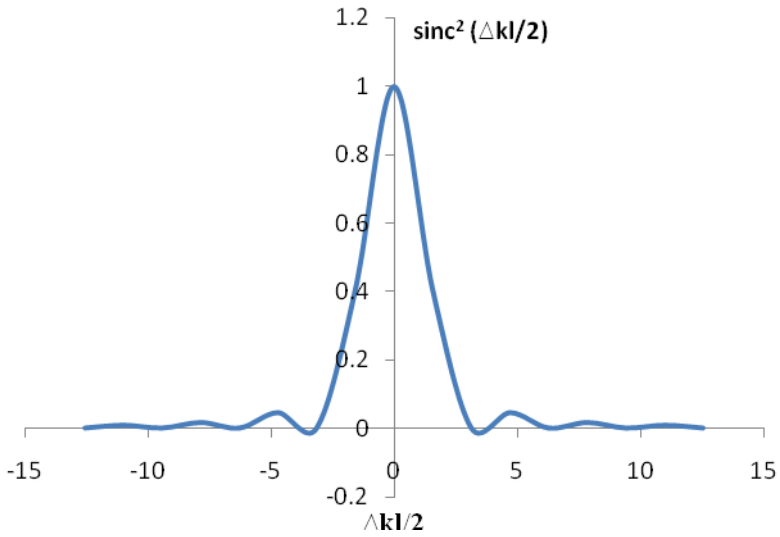

Figure 9 Sinc^2 Function

For perfect phase matching (Δk=0), equation (2) above can be re written as

$$I_{2w}(l) = \frac{2\pi^2 d_{eff}^2}{\lambda_w^2 n_{2w} n_w^2 \varepsilon_0 c} l^2 I_w^2 \qquad (3)$$

In practical terms, this means that for a useful frequency doubled beam to emerge from the crystal, it is essential that the second harmonic light generated at each point along the crystal's length interferes constructively with the existing wave. This happens when the phase velocity of the fundamental and the second harmonic waves are equal. This is an important condition which must be met for efficient frequency conversion and is known as phase matching.

The most frequently used technique for phase matching is to make use of the birefringent properties of the material, the fact that many crystalline materials are characterised by two refractive indices. The refractive index experienced by a wave propagating through the material depends on the direction of propagation and direction of polarisation relative to the crystal symmetry axis. A wave is said to be ordinary if it is propagated with its polarisation perpendicular to the optic axis. The refractive index seen by the wave is n_o, independent of the direction of propagation. A wave is said to be extraordinary if it has a component of the polarisation along the optic axis. The refractive index seen by the wave in this case depends on the direction of propagation, varying continuously from n_e when it propagates perpendicular to the optic axis to n_o as the propagation direction approaches the optic axis.

Consider the situation where the fundamental wave is launched as an ordinary wave and the second harmonic is generated as an extraordinary wave. If

$n_e(2\omega) \leq n_o(2\omega)$ $n_o(2\omega)$ the refractive index can be tuned to any value between $n_e(2\omega)$ and $n_o(2\omega)$ and in particular $n_o(2\omega)$, where $\Delta k=0$. The phase matching angle θ_m is the angle of propagation where the index of refraction of the extraordinary second harmonic wave equals that of the ordinary fundamental, as illustrated in Figure 10.

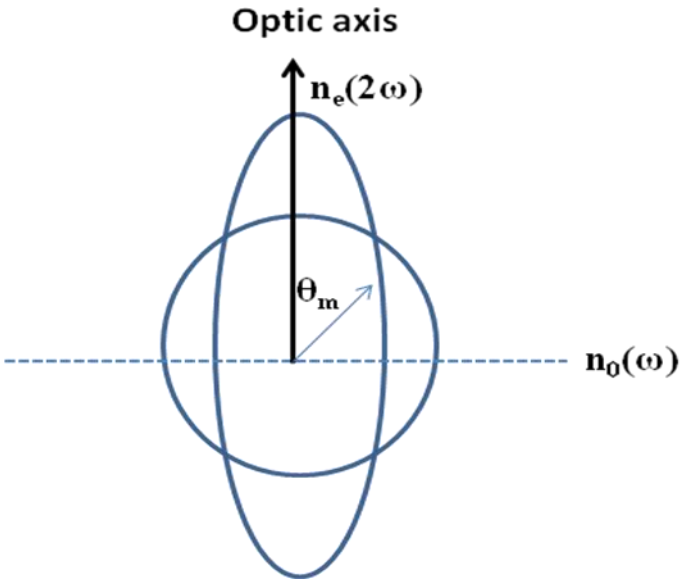

Figure 10 Birefringent phase-matching

In most cases of SHG, the frequency doubled light will propagate spatially separated from the fundamental beam. This is known as walk-off and is highly undesirable as it leads to poor beam quality and low conversion efficiency. This effect is prevented with non-critical phase matching which is the special case of birefringent phase matching where θ_m=90 degrees as shown in Figure 11.

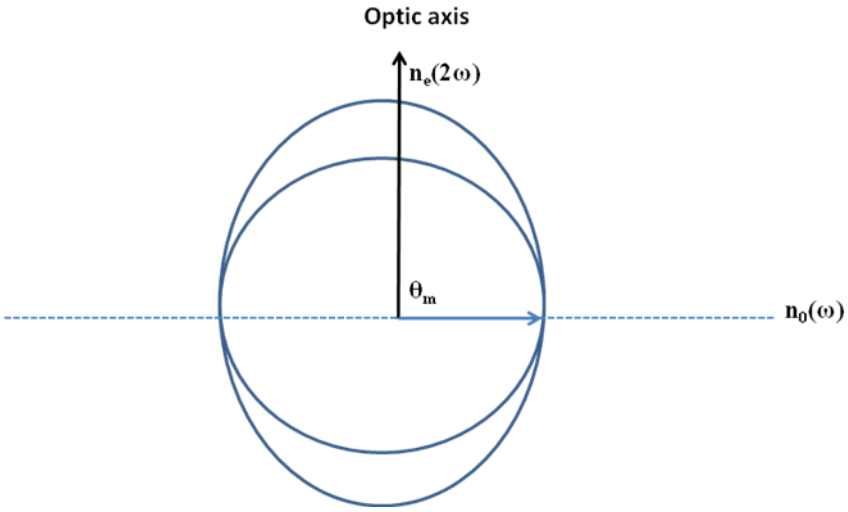

Figure 11 Non-critical phase-matching

For non-critical phase matching the birefringence exactly matches the dispersion at one particular temperature, and so the phase matching is temperature tuned. In the following experiments SHG of the 980nm VECSEL output is performed using potassium niobate ($KNbO_3$) which was B-cut for non-critical phase matching at a temperature of 10 degrees.

Pump Depletion

Mathematically, there is nothing in equation (3) to prevent the second harmonic intensity exceeding that of the fundamental if the input power is made large enough and the crystal length is long enough. Physically however, this situation violates the fundamental law of conversion of energy.

The flaw is, that, one major assumption of the above equation is the amplitude of the fundamental field remains constant throughout the SHG process, however as the process is converting power from ω_1 to $2\omega_1$, the build up of power at the second harmonic must eventually begin to deplete the fundamental.

This problem is treated in far more detail by [7] where the solution is presented by describing the growth of the intensity of the second harmonic, $I_{2w}(l)$ according to the following equation

$$I_{2w}(l) = I_w(0)tanh^2(\Gamma l) \qquad (4)$$

where $\Gamma = A_1(0)\sqrt{\frac{\kappa_1}{\kappa_s}}$, where $\kappa_i = \frac{k_i d_{eff}}{n_i^2}$ and $A_1(0)$ is the initial amplitude of the fundamental plane wave. This function is shown in Figure 12.

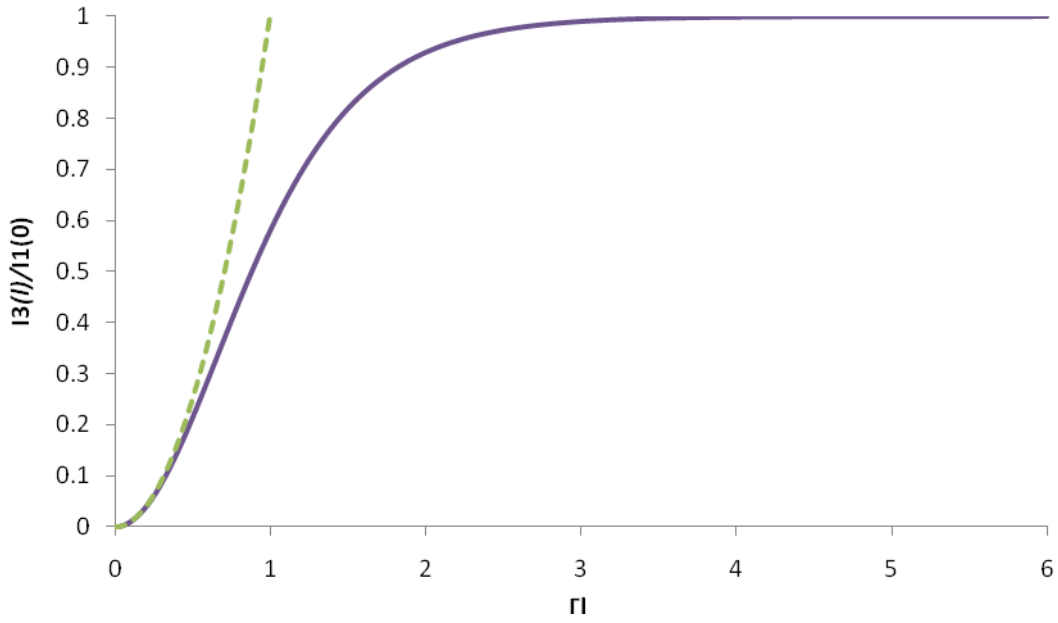

Figure 12 Second harmonic efficiency with pump depletion considerations (The dashed curve shows the quadratic "no-depletion" approximation)

This shows that by taking into account pump depletion effects, the second harmonic efficiency $I_{2w}(l)/I_w(0)$ cannot exceed unity, and therefore conservation of energy is not violated. In the low conversion efficiency regime (Γl <<1), $\tanh^2(\Gamma l)$ is approximately $\Gamma^2 l^2$ and the curves overlap. From Figure 12, it can be seen that the low efficiency regime approximation is suitable up to ~10% conversion efficiency.

Optimisation of Second Harmonic conversion efficiency

Until now, the theory presented for SHG has assumed a plane wave fundamental input. However in practice the lasers used in nonlinear frequency conversion experiments emit 'real' beams, described by Gaussian optics, in which the emission lineshape is represented by a Gaussian shaped intensity distribution.

The VECSEL laser source used in the following experiments emits in a near diffraction- limited (fundamental transverse mode TEM_{00}) Gaussian beam.

The expected SHG power generated by a TEM_{00} diffraction limited Gaussian beam is given by

$$P_{2w} = 1.068 \frac{16\pi^2 d_{eff}^2}{\lambda_w^3 n_w n_{2w} c\epsilon_o} l P_w^2 = \gamma_{SHG} P_w^2 \qquad (5)$$

Equation (5) states that the generated second harmonic power depends on the square of the fundamental power and the interaction length of the propagating beam in the crystal. It is therefore necessary to have the fundamental propagating beam tightly focussed at the centre of the crystal to give a high intensity. However a reasonable interaction (i.e crystal) length is also required.

As a tightly focused Gaussian beam is subject to diffraction, a trade off between high intensity and long interaction length in order to achieve efficient second harmonic conversion efficiency is introduced.

To overcome this, an optimum ratio of the interaction length (l) to longitudinal extent of the focal region (b) of l/b=2.84 [9] has been determined for SHG of TEM_{00} diffraction-limited Gaussian beams

According to the Boyd and Kleinman theory [9], under optimum focusing conditions the spot size $\omega_{0,}$ of a TEM_{00} diffraction- limited Gaussian fundamental beam, inside a non-critically phase-matched crystal is given by

$$\omega_0 = \sqrt{\frac{\lambda_w l}{2\pi n_w 2.84}} \qquad (5)$$

where l is the crystal length, n_w is the refractive index seen by the fundamental beam, and λ_w, the wavelength of the fundamental.

In all of the following experiments optimum focusing into the crystal is considered.

Sum Frequency Generation

Sum frequency generation (SFG) is the nonlinear process whereby two pump beams at frequencies ω_1 and ω_2, generate a beam at a frequency of the sum of the pump beam frequencies $\omega_1 + \omega_2$. This process is illustrated in Figure 13.

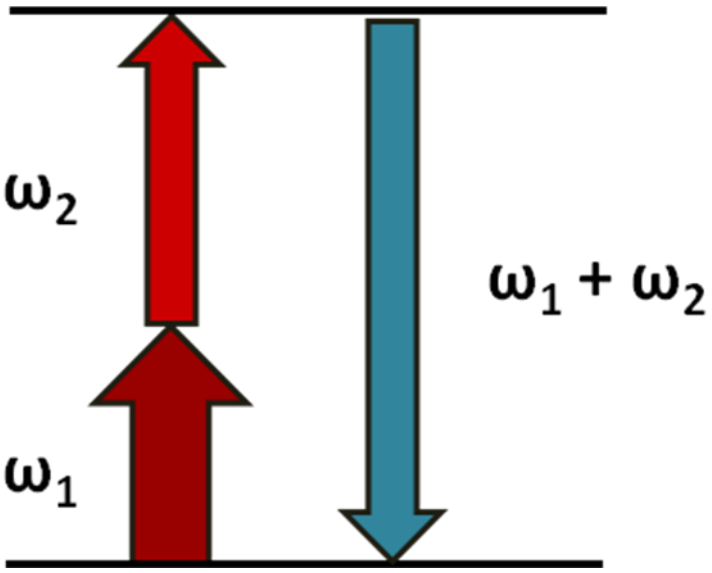

Figure 13 Sum Frequency Generation

As with SHG this process occurs in crystal materials which exhibit a $\chi^{(2)}$ nonlinearity, and requires accurate phase matching and optimum focusing for efficient frequency conversion.

Schemes to produce blue light, as is presented in this thesis, often mix a very strong pump beam at wavelength λ_2, with a much weaker probe at λ_1. In an ideal case, with optimum focusing and phase matching, all of the power present in the weaker beam would be converted into blue light at wavelength λ_3.

The theory of SFG first presented by [11] shows that the intensity of the generated sum frequency wave, $I_3(l)$, at the end of the nonlinear crystal, of length l, can be written as

$$I_3(l) = \frac{\lambda_1}{\lambda_3} I_1(0) sin^2\left(\frac{\pi}{2}\frac{l}{l_{max}}\right) \qquad (7)$$

where $l_{max} = \pi/2\sqrt{\kappa_1}\kappa_3$ where $\kappa_i = k_i d_{eff}\sqrt{2\eta_2 I_2(0)}/n_i^2$ is the length at which the maximum sum-frequency intensity is produced. The intensity of the weaker probe $I_1(l)$ varies as

$$I_1(l) = I_1(0)cos^2(\frac{\pi}{2}\frac{l}{l_{max}}) \qquad (8)$$

The variation of $I_1(x)$ and $I_3(x)$ is shown in Figure 14. Although it may look like energy conservation is being violated, $I_3(x) > I_1(0)$, because the generated wave also extracts power from the second, stronger pump beam at ω_2.

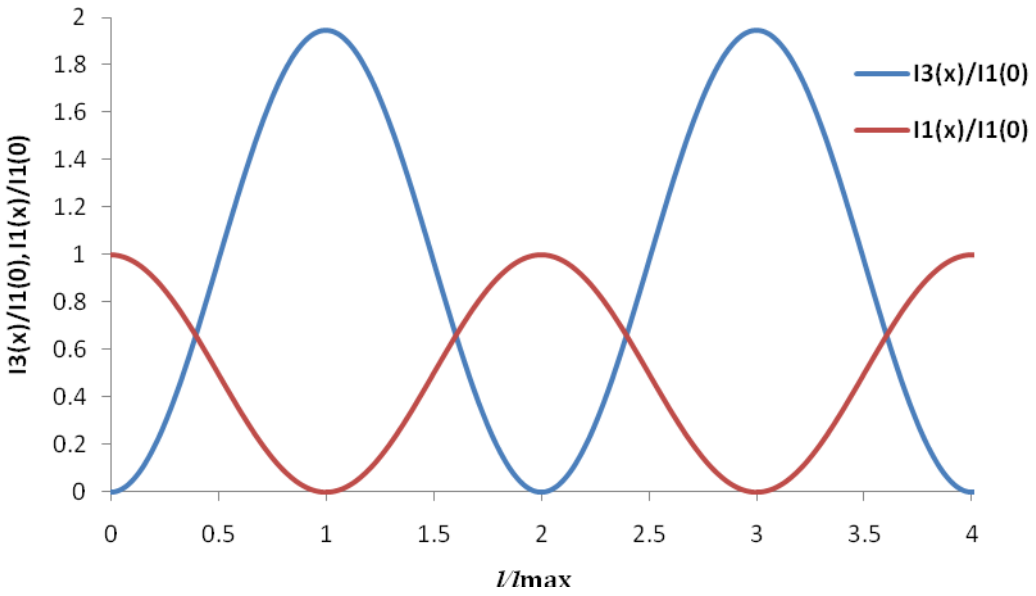

Figure 14 Variation of the relative power in the weaker pump wave at ω_1 and the generated sum frequency wave at ω_3 versus interaction length

Conclusion

A brief overview of the basic principles of nonlinear optics has been presented. This has included a detailed description of two nonlinear processes; second harmonic generation and sum frequency generation which are to be the focus for the work in this thesis. Also included was a discussion on increasing the optical conversion efficiency by means of phase matching and optimisation of the focussing inside the crystal.

References

[1] Maiman T.H., Stimulated optical radiation in Ruby, Nature, **187**, 1960, 493

[2] Eppler W.R., Kryder M.H., Garnets for short wavelength magneto-optic recording, J Phys Chem Solids, **56**, 1995, 1479

[3] Glenn W.E., Dixon G.J., Bright future projected for lasers in electronic cinemas, Laser Focus World, November**,** 1993, 73

[4] Bjorklund G.C., Frequency-modulation spectroscopy: a new method for measuring weak absorptions and dispersions, Opt Lett, **5**, 1980, 15

[5] Sklar L.A., Lasers in flow cytometry and biotechnology, Compact Blue Green Lasers Technical Digest, **6**, 1992, 8

[6] Franken P.A., Hill A.E., Peters C.W., Weinreich G., Generation of optical harmonics, Phys Rev Lett, **7**, 11, 1997, 1417

[7] Compact Blue-Green Lasers, Risk, Gosnell & Nurmikko, published by Cambridge University Press, 2003

[8] Feynman R.P., Leighton R.P., Sands M., The Feynman Lectures on Physics, Volume I, 1993

[9] Boyd G.D., Kleinmann D.A., Parametric interaction of focused Gaussian light beams, J Appl Phys, **39**, 1968, 3597

[10] Ashkin A., Boyd G.D., Dziedzic J.M., Observation of continuous optical harmonic generation with gas masers, Phys Rev Lett, **11**, 1963, 14

[11] Bass M., Franken P.A., Hill E.A., Peters C.W., Weinreich G., Optical Mixing, Phys Rev Lett**, 8**, 1, 1962,18

Chapter 3 Characterisation of the VECSEL Source

VECSEL Gain Chip

The VECSEL gain chip used in this work was designed for emission at 980nm when optically pumped at a peak absorption wavelength of 808nm, to provide an output peak at 490nm when frequency doubled. These wavelengths were specifically chosen at the design stage, where the bandgaps of the quantum wells have been engineered to provide absorption and emission at the desired energy. The pump wavelength was chosen to capitalize on the widely available, low cost, 808nm diode lasers.

Optical Pump Analysis

The size and intensity profile of the pump beam incident on the VECSEL surface plays a crucial role in ensuring good beam quality and efficient output of the laser [1].

The size of the pump beam should be matched in size to that of the fundamental cavity mode (determined by the cavity geometry). If the beam is too large then it will provide sufficient optical power to excite the extremes of the cavity mode which can lead to unwanted, additional higher order transverse modes oscillating inside the cavity, This can result in poor beam quality and instabilities in the laser output. However, if it does not pump a sufficient surface area, excess losses will be incurred and lasing may not be achieved.

It is also important to consider the intensity profile that the pump beam provides. This should be matched to that of the beam circulating in a VECSEL cavity, which is described by a Gaussian profile.

The source used for optical pumping of the VECSEL in the following experiments is an 808nm fibre-coupled laser diode (Optotools) emitted from a 100µm fibre, which

is focused down inside the gain medium (to a spot size ~100µm) using a homemade lens package consisting of two 25mm focal length achromatic doublet lenses separated by 40mm, with the first lens 26.75mm from the fibre output.
This source can provide up to 7W of power but under normal operating conditions it provides ~5W of optical pump power to the VECSEL source.

To analyse the pump beam size and corresponding output intensity profile a Coherent Lasercam III beam analyser was used with a 10X microscope objective lens fitted at a fixed distance from the imaging head of the camera(to magnify the small pump beam diameters to the required camera resolution). The modified system was calibrated by imaging a series of pinholes of know diameter, and a correction factor was applied to the diameter measurements to correct for the beam propagation through the fixed distance from the 10X microscope objective and the camera imaging system.

Measurements of the pump beam diameter at the focus and its corresponding intensity profile at various distances from the pump focal point were taken as shown in Figure 15 and the results are shown in Figure 16**.**

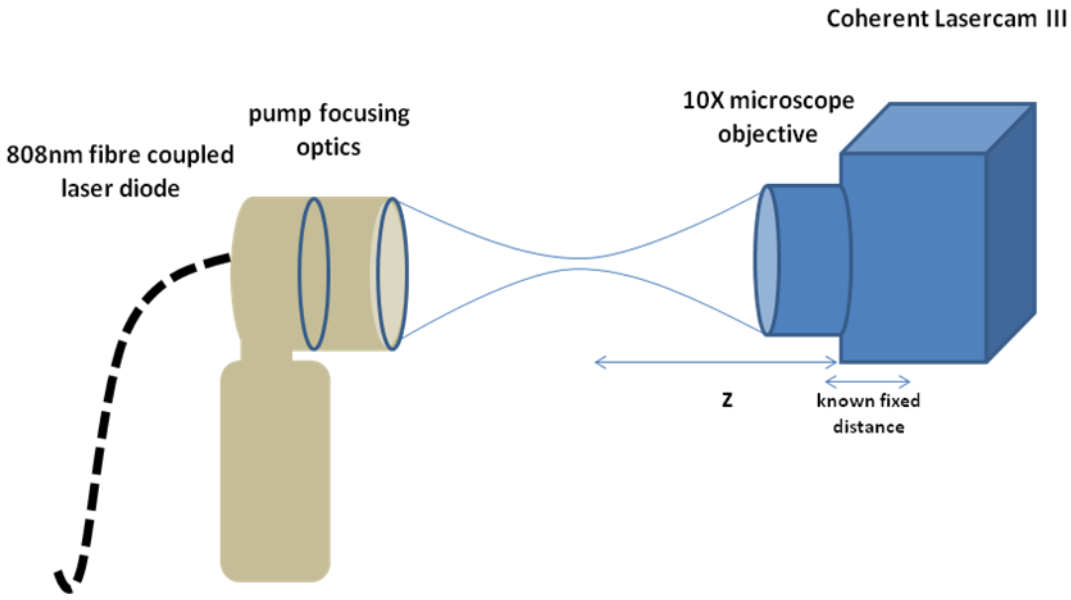

Figure 15 Pump profile analysis experiment

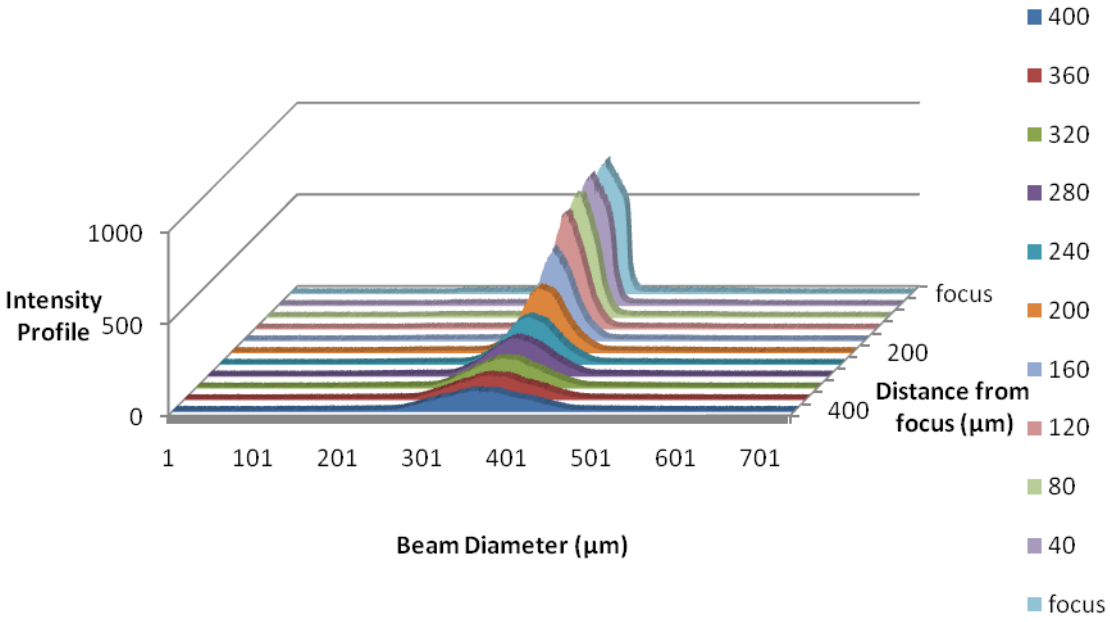

Figure 16 **Pump beam profile near to the focus**

It can be seen that for distances at, and close to the focus, the beam diameter is small and the intensity profile exhibits a sharp peak with a quick fall off on either side.
As the distance is increased from the focus, the beam diameter expands and takes on a smoother profile, as seen ~200µm from the focus. At this point the beam diameter is 120µm, which provides a good match for cavity modes circulating insides cavities of ~1m round-trip length, which is the expected practical working distance of the VECSEL cavity in the following experiments.

External Cavity Configuration

The DBR forms the end mirror in a linear folded cavity completed by the addition of a curved high reflector and a flat output coupler, as shown in Figure 17.

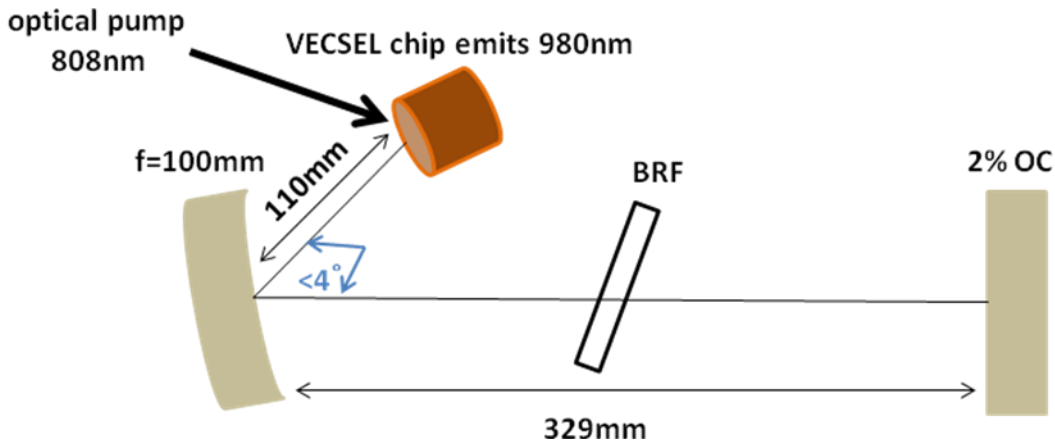

Figure 17 External cavity schematic

The VECSEL chip is held in a copped mount which is water cooled temperature of 10 degrees.

The external cavity was designed using WinLase software, which models Gaussian beam propagation using ABCD matrices. The mirror radius of curvature and the separations were chosen to ensure a stable cavity for which the cavity mode matches the pump spot size (as discussed earlier), and with sufficient length in the collimated arm to accommodate a birefringent filter and an etalon, for wavelength selection and tuneability.

A birefringent filter is made from the birefringent material quartz and is cut at Brewsters angle for low insertion loss. The birefringence of the material acts to separate the ordinary and extraordinary polarisation components of the beam incident on it, as each component experiences a different refractive index, resulting in two rays with different phase velocities. Only the rays for which the path length equals an

integral multiple wavelengths are transmitted through the filter. Low losses occur for integral orders of full waves, producing a comb like transmission spectrum. A slight rotation of the BRF allows the laser to translate the wavelength of the transmission peaks and therefore tune the output wavelength of the source [2].

Figure 18 models the evolution of the beam radius with distance from the VECSEL chip surface for the cavity geometry. The cavity defined beam radius at the VECSEL surface is ~80µm therefore providing a good theoretical match between the cavity spot size and the optimal pump beam diameter, as discussed previously. The beam emerging from the VECSEL cavity has a radius of 361µm.

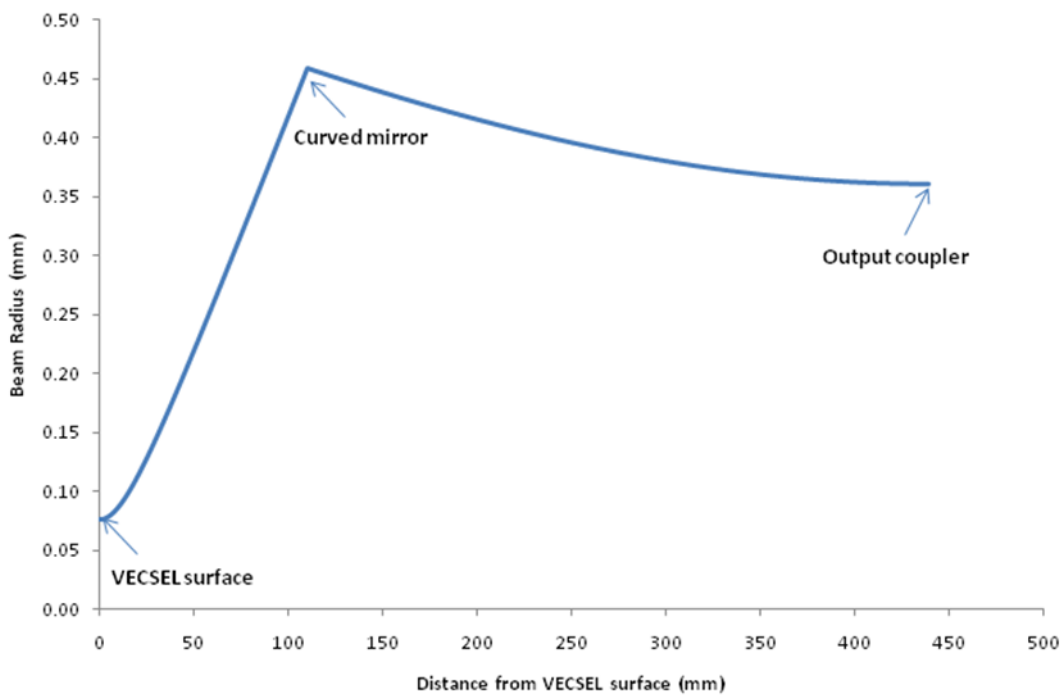

Figure 18 Evolution of the cavity defined beam radius with distance from VECSEL surface

The opening angle of the curved mirror was kept to a few degrees in order to minimize astigmatism within the cavity.

Figure 19 shows the range of distances from the VECSEL chip to the curved mirror for which the cavity is stable, illustrated as stable for values $0<y\leq1$ for the tangential

component and -1≤y<0 for the sagittal component of the beam circulating within this cavity geometry.

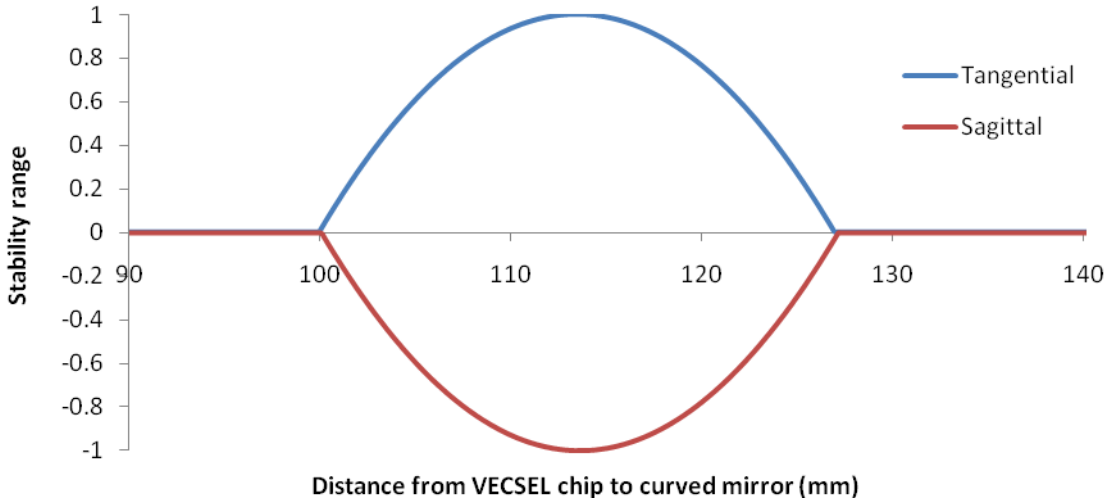

Figure 19 Cavity stability range for our cavity geometry with opening angle < 4 degrees

The overlap of both ranges indicates minimal astigmatism and therefore, a stable cavity geometry. It can be seen from Figure 20 that when the opening angle is increased to 20 degrees the overlap between the components separates, which will result in a highly astigmatic cavity which gives an elliptical output beam and is very sensitive to critical alignment.

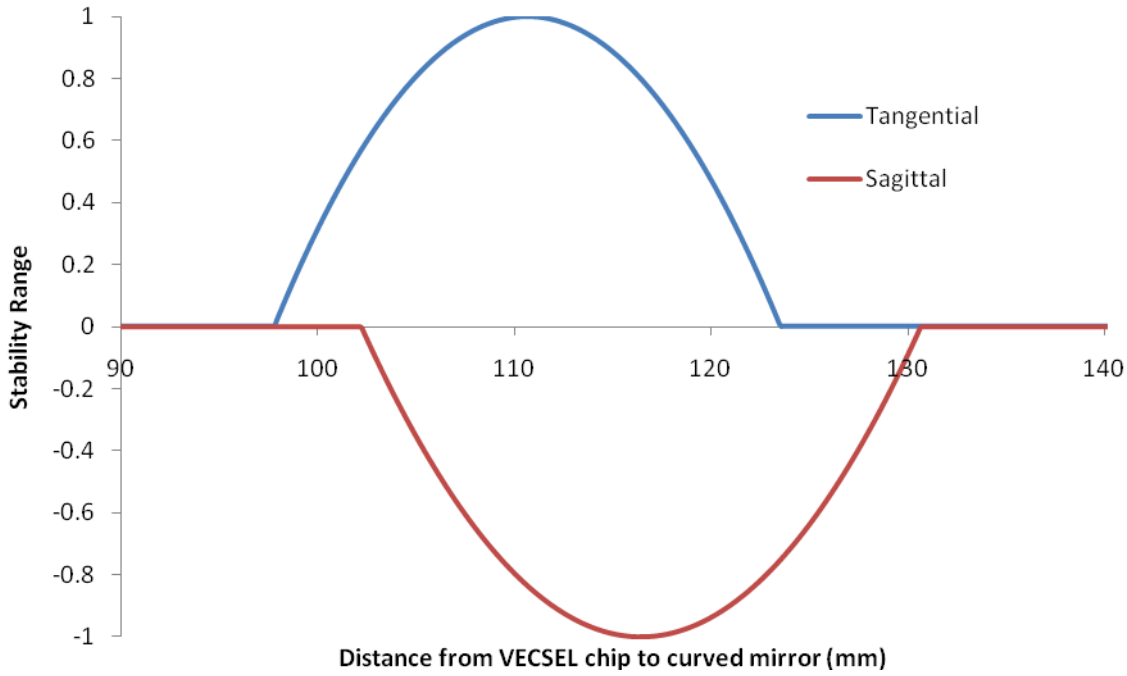

Figure 20 Cavity stability range for our cavity geometry with opening angle ~10 degrees

Various output coupling transmissions were tested and the optimum was determined to be 2%.

Output Power

Shown in Figure 21 is the generated VECSEL power as a function of input pump power.

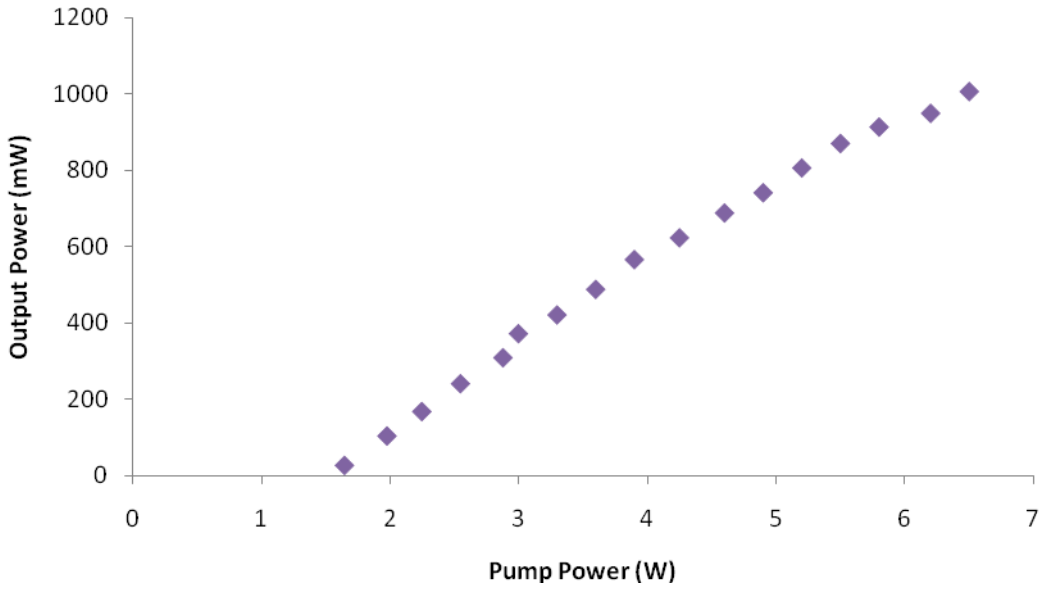

Figure 21 **VECSEL power curve**

The laser output has a maximum power in excess of 800mW and a threshold pump power of 1.5W.

Above threshold, optical pumping powers up to 4.5W result in a efficiency response of the source of ~30% . Above 4.5W of optical pump power the slope efficiency of the VECSELs response is reduced to ~20%. Increasing the pump power eventually leads to a thermal rollover situation in which the output power of the source saturates. By extrapolation of the data points in Figure 21 we can see that this happens for pump powers exceeding 8W, which is out with the maximum power levels provided by our pump source.

The data presented above represents the inclusion of the BRF inside the external cavity. Without the BRF the laser output exceeds 1W and has a threshold pump power of 1.2W, but in this situation the tunability of the source is compromised.

Tunability

The birefringent filter inside the external cavity was rotated to provide various output wavelengths for the VECSEL beam (monitored using a USB2000 spectrometer) at an optical pump power of 5W, and the output power at each wavelength was measured.

The gain medium of the VECSEL supported a tuning range of 20nm as shown in Figure 22.

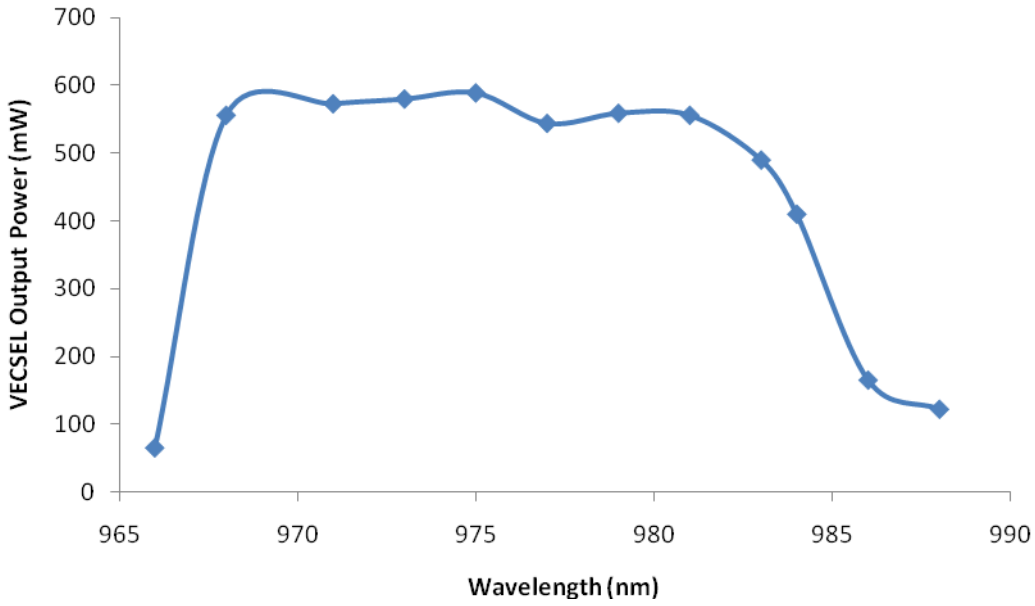

Figure 22 VECSEL output tuning range

Beam Quality

To quantify the quality of the output laser beam, the M^2 parameter was used. The M^2 parameter describes how far the beam intensity profile deviates from that of a perfect fundamental Gaussian (i.e. TEM_{00} where $M^2=1$) [3].

The beam radius, w(z), was measured (using a Thorlabs BP100 beam profiler) as a function of distance, z, from the focus. For a diffraction limited beam (TEM_{00}) the beam radius, w(z), evolves according to the equation;

$$\omega(z)^2 = \omega_0^2 + (\frac{\lambda}{\pi\omega_0})^2 z^2 \qquad (9)$$

where ω_0 is the minimum spot size and λ the wavelength of light, in this case 980nm. If however, the beam contains proportions of higher order modes it will diffract more rapidly for a given minimum spot size. This is described by the M^2 parameter;

$$\omega(z)^2 = \omega_0^2 + M^4(\frac{\lambda}{\pi\omega_0})^2 z^2 \qquad (10)$$

Using a least squares comparison method the actual and the perfect Gaussian beam radii can be compared and the M^2 value obtained.

The results for the beam profile measurements plotted alongside the evolution of a diffraction limited beam (M^2=1) for the same focused spot in the described cavity configuration are shown in Figure 23.

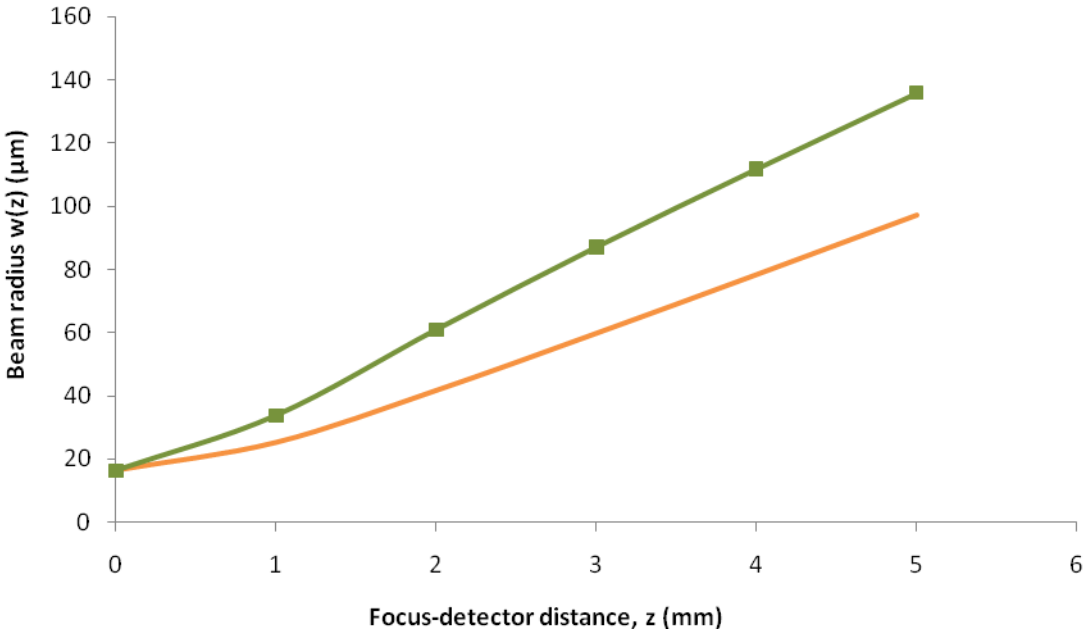

Figure 23 Evolution of the beam radius of the VECSEL output. The smooth orange curve indicates the evolution of a diffraction limited beam (M^2=1) for the same focused spot size.

The M^2 value obtained for the VECSEL was 1.4 indicating a good quality beam which is reasonably close to diffraction limited.

The M^2 value for a range of various cavity geometries was investigated. These ranged from M^2 values of 1.05 indicating excellent beam quality in a very near diffraction limited beam to some very poor quality beams with M^2 values exceeding 2.

Although the cavity used in this experiment did not represent the best M^2 value obtained, it did represent the best cavity geometry in terms of available space in the long arm for insertion of the BRF and other optical elements, it produced a good sized cavity mode which could be matched to the pump beam diameter, and it provided the most suitable roundtrip length which was important for exact matching to the external resonator cavity in later experiments.

Polarisation

The polarisation of the VECSEL output was determined, using a polarising beam splitter, to be linearly polarised in the horizontal plane (i.e parallel to the table).

Conclusion

The laser produced a good quality output beam with a tuning range of ~20nm and high powers in excess of 800mW.

References

[1]Gardner K.S., Single Frequency Vertical External Cavity Surface Emitting Lasers, PHD Thesis, University of Strathclyde, 2007

[2] Bloom A.L., Modes of a laser resonator containing tilted birefringent plates", J. Opt. Soc. Am. **64** (4), 1974, 447

[3] A. E. Siegman, Tutorial, Optical Society of America Annual Meeting, 1997 unpublished

Chapter 4 Confocal Laser Scanning Microscopy using a frequency doubled VECSEL

Introduction

Confocal laser scanning microscopy (CLSM) is a light microscopy technique in which only small area sections of a sample are observed at one time and an overall image is then constructed through point by point scanning of each of these small area sections over the whole sample.

This sophisticated new technique offers many advantages over conventional optical microscopy including, the ability to control depth of field, a reduction in unwanted image degradation background, and the capability to collect optical sections from thick specimens therefore providing sharper 3D images.

There has been an explosion in the popularity of CLSM in recent years due in part to the relative ease with which high-quality images can be obtained from specimens prepared for conventional fluorescence microscopy, and the growing number of applications in cell biology that rely on imaging both fixed and living cells and tissues [1]

When imaging fluorescent live cells and tissues in CLSM, judicious choice must be given to the excitation laser source to be used. By matching the emission wavelength range of the excitation source to the absorption spectrum of the fluorescent label or peak reflection wavelength of the sample, good quality high resolution images can be obtained whilst minimising detrimental photodamage and thermal loading effects.

The argon ion laser, at wavelength 488nm, is at present the most common laser used for reaching the blue wavelength range in CLSM due to its wide availability and relative reliability. However this laser can only operate at a few defined wavelengths and is therefore not a tunable source, meaning that it is unsuitable for excitation of various types of fluorescent dye.

Also, the use of this source presents several limitations for quantitative analysis of CLSM images. Firstly, this heavy, bulky system comprises a discharge-based gain

medium which typically exhibits high amplitude noise levels. Furthermore, this system lacks tuneability of wavelength, severely restricting the fluorescent dyes and samples which can be imaged. Additionally, the stability of argon ion laser is dictated by the environmental operating conditions which, when subject to externally induced fluctuations, can severely limit the achievable resolution of the CLSM images.
Hence, an alternative low-cost, compact, wavelength tuneable, stable and reliable solid state system is sought for CLSM.

A frequency doubled 980nm VECSEL has the potential to present as an attractive replacement for the argon ion laser for applications in CLSM. VECSELs can offer the precise wavelength tailoring and tunability aspects required for these applications as well as being relatively low cost, compact, robust and reliable.

This chapter presents a frequency doubled 980nm VECSEL as an alternative blue wavelength source for applications in CLSM.

Experiment

Single pass second harmonic generation (or frequency doubling) of the VECSEL output (as described in the previous chapter) was performed using the nonlinear crystal potassium niobate ($KNbO_3$). $KNbO_3$ is an attractive material in nonlinear optics due to its high nonlinearity, and its ability to noncritical (90 degree) phase match via temperature tuning thus eliminating walk off of the generated beam. The crystal dimensions were 3x3x10mm and AR coating was applied at 980nm and 490nm on both surfaces to reduce reflection losses.

The crystal was B-cut for type I phase matched SHG of 980nm measured at an optimum temperature of ~10 ºC, as shown in Figure 24, and has an effective nonlinear coefficient d_{eff} =9.25pm/V.

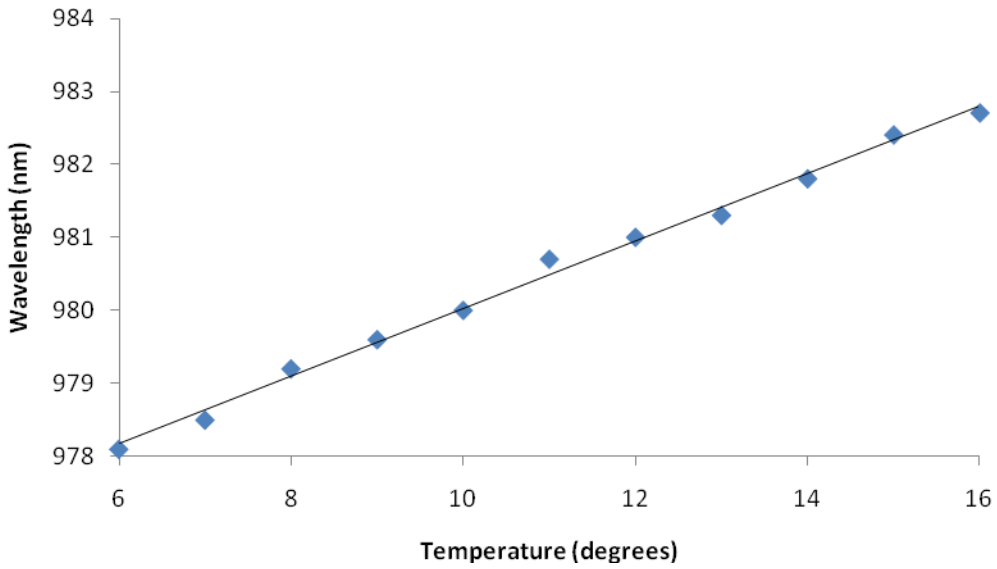

Figure 24 Non-critical phasematching in $KNbO_3$. The data points represent the experimentally measured values and the solid line is the theoretically expected phasematching curve [2].

This temperature was achieved by mounting the crystal in a water cooled copper block maintained by the same chiller, at the same temperature as the VECSEL mount. The application of a single cooling system significantly simplified and reduced the power consumption of the overall system.

The output beam of the VECSEL was focused into the $KNbO_3$ crystal as shown in Figure 25. The optimum focused spot size determined by the Boyd-Kleinmann focusing parameter (as described in Chapter 2) for refractive index n=2.225 (calculated using the Sellmier equations and nonlinear coefficients provided by Umemura et al [2]) was w_o=15.6μm, located exactly halfway along the crystal's length. This calculation assumed a diffraction limited fundamental beam with a calculated expected second harmonic power P_{490}=2.2mW for a fundamental power P_{980}=400mW.

For the VECSEL cavity described in Chapter 3, this focusing was achieved using an f=+40mm focal length lens placed 85mm from the output coupler as shown in Figure 25. The generated beam was then collimated with a f=+80mm lens, chosen to

provide a spot size of w=2μm at the system input, in order to overfill the microscope objective back aperture, maximising the resolution of the resulting images.

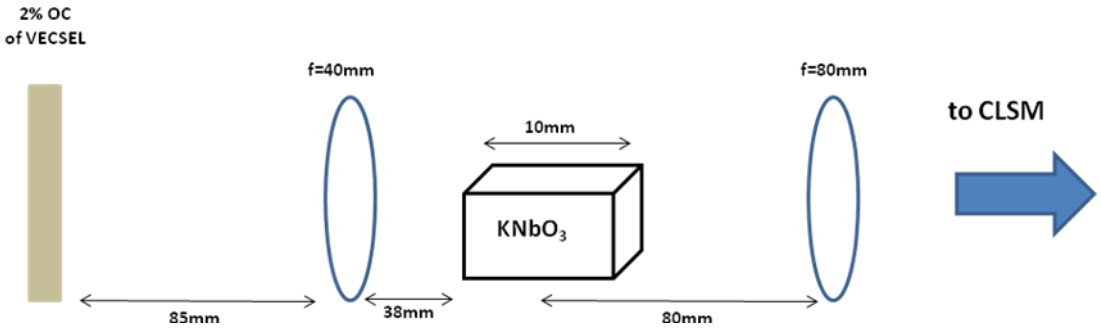

Figure 25 VECSEL frequency doubling

Characterisation of the Source

The second harmonic output was optimised at a fundamental laser wavelength of 980nm and power of 540mW, providing approximately 1.8mW of SHG power measured at a wavelength of 490nm.

The dependence of the SHG power on the VECSEL power is shown in Figure 26

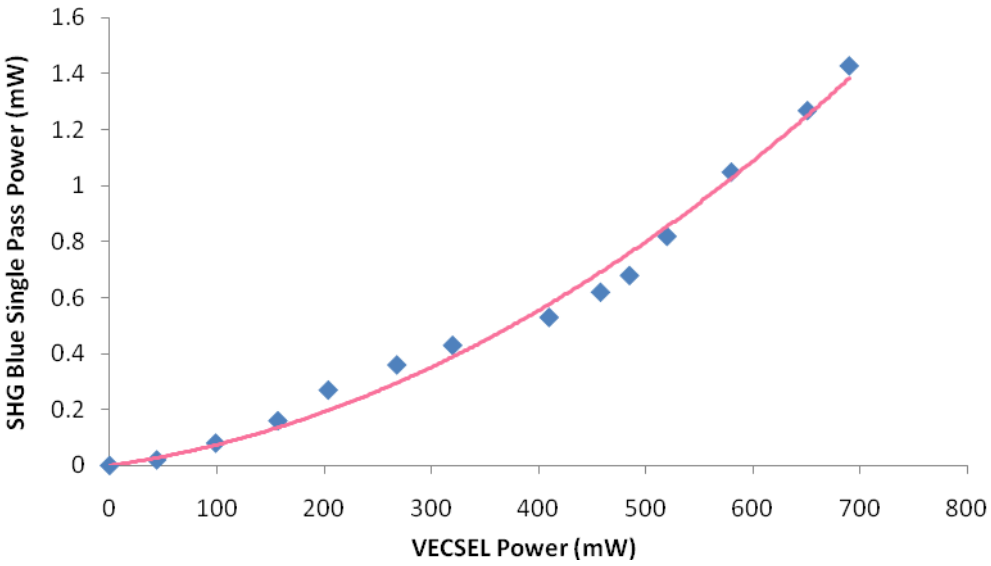

Figure 26 Blue output power dependence on VECSEL input power. The diamonds indicate the experimentally obtained measurements and the solid line is the parabolic fit to the data.

As expected, the SHG power depends quadratically on fundamental laser power.

The slightly lower than expected second harmonic power was attributed to the laser beam being slightly above the diffraction limit and potentially to imperfections in the crystal. However, as demonstrated below, the overall power level was still ample for CLSM imaging.

The second harmonic beam quality at 490nm was measured using the M^2 parameter (as described in Appendix A). Along both axes of the beam, the measurements are consistent with an M^2 value of ~1.35 which compares well with that of other solid-state sources used in microscopy applications [3], and hence we could anticipate high-resolution CLSM images.

Imaging

To evaluate the efficacy of the frequency doubled source for CLSM, the developed source was coupled into an Olympus Fluoview FV1000 CLSM system.

A half-wave plate was inserted into the beam path to adjust the polarisation of the source relative to the polarisation dependent elements contained in the microscope system.

Figure 27 contains images produced with the frequency doubled VECSEL providing <1mW at the sample using an Olympus 40x 0.9 NA air objective.
Each sample has been labelled with dyes which have a peak excitation ~490nm.

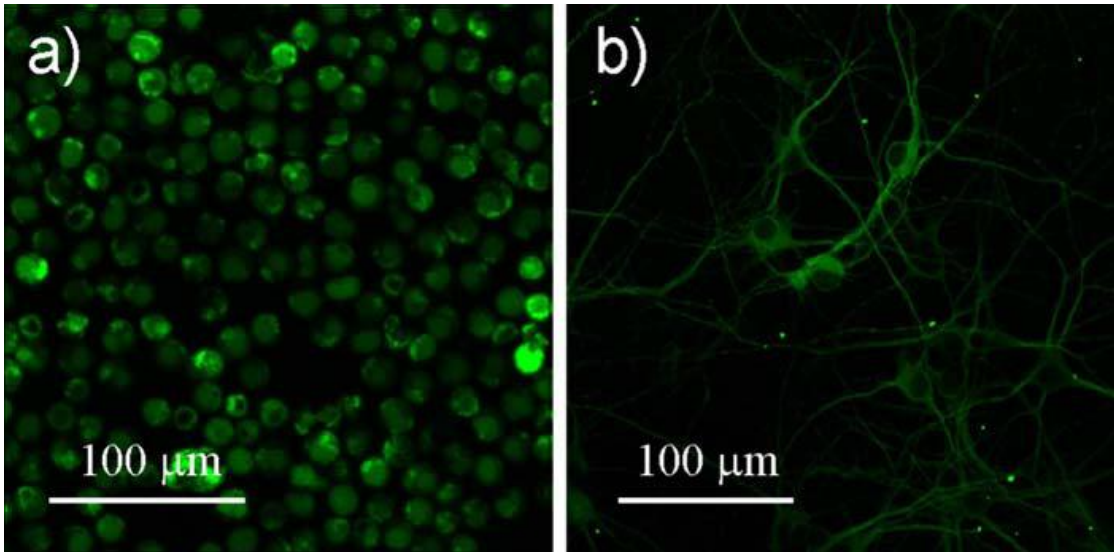

Figure 27 CLSM Images produced with frequency doubled VECSEL (a)T-lymphocytes labelled with green fluorescent dye (CFSE) and (b) rat hippocampal neurons labelled with Alexa Fluor 488

Fluorescently labelling the presented cells allows them to be used in many studies, including the dynamic cell-cell interactions of the mammalian immune system [4].

Figure 28 shows the same sample recorded with the frequency doubled VECSEL and a standard argon ion laser (Melles Griot IMA101040ALS). The images were taken at comparable average power.

Comparison of the figures highlight that in terms of image quality, both lasers give similar results however, the argon ion laser exhibits a lower signal to background ratio than the VECSEL. This can compromise the integrity of the resultant image and subsequent analysis, thus leading to increased errors in quantitative measurements from the CLSM images.

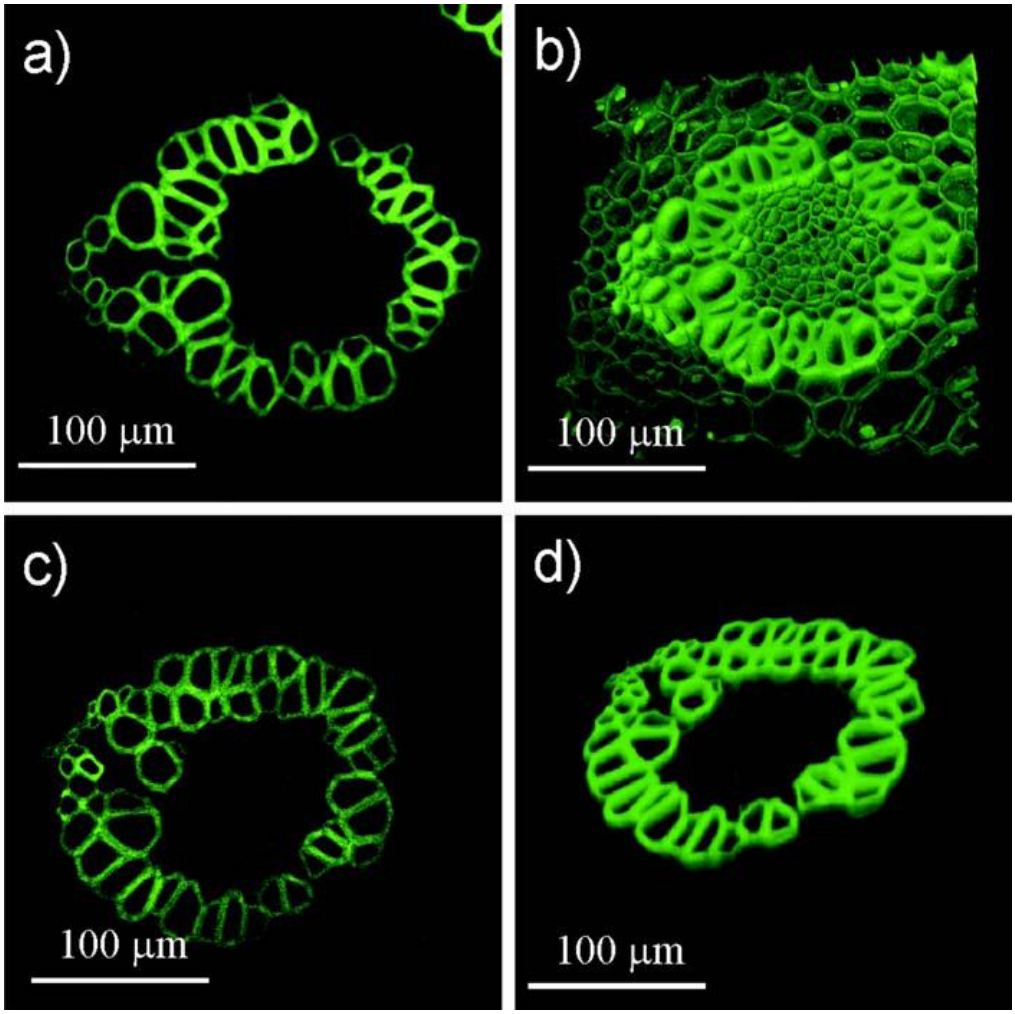

Figure 28 CLSM images taken of convallaria (Lily of theValley) (a) and (b) were obtained using the frequency doubled VECSEL, whereas (c) and (d) were captured using an argon ion laser.
Images (a) and (c) are transverse sections of rhizone with concentric vascular bundles; images (b) and (d) are 3D reconstitutions of stacks from the convallaria rhizone section.

In order to assess, quantify and compare in greater detail, the level of laser system noise for both sources each output beam was sent to a spectrometer (Ocean Optics USB2000). The spectrometers recorded the intensity of the sources in a 1nm bandwidth. The intensities were acquired continuously and simultaneously over a 60s period with 50μs resolution. The data presented in Figure 29 is a plot of the normalized intensity variations for both the frequency doubled VECSEL and the argon ion laser over a 60s period.

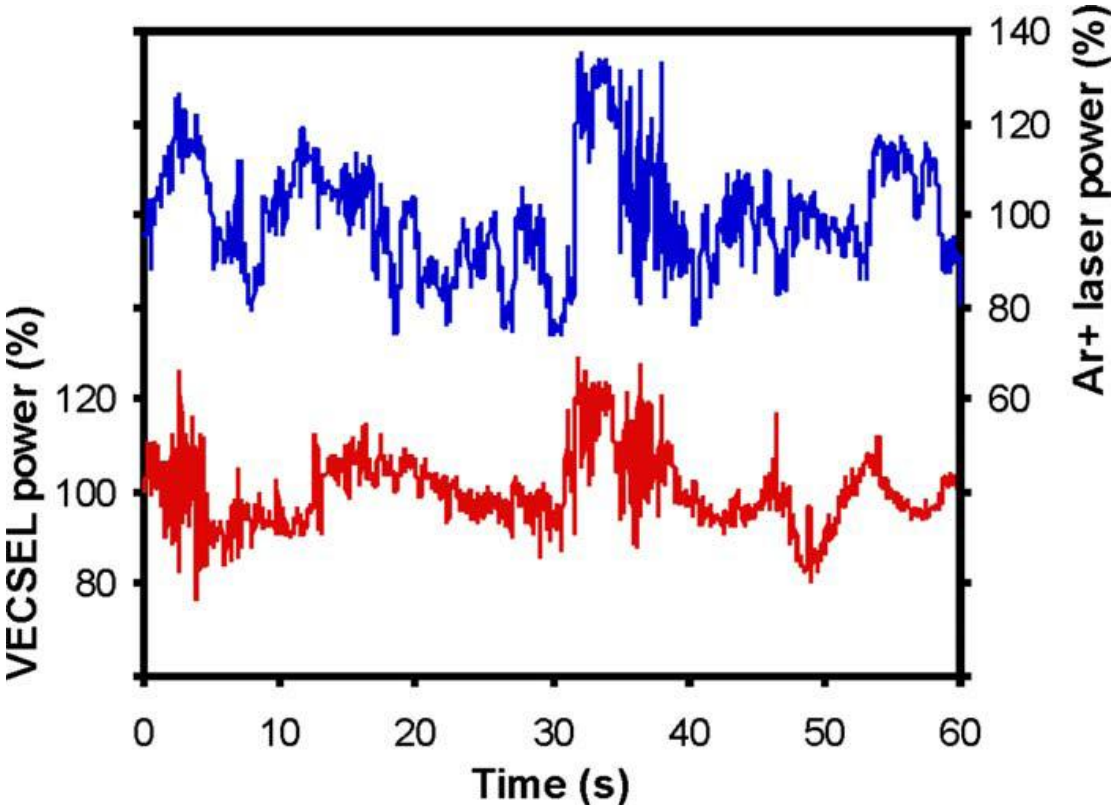

Figure 29 **Comparison of the intensity noise between the frequency doubled VECSEL and an argon ion laser.**

The correlation between the noise levels in the two simultaneously recorded traces suggests that the noise experienced by both sources is affected to a large extent by the environmental surroundings, and the observations imply that the argon ion laser is more susceptible to such perturbations. This is evident from the large fluctuation from which both sources respond to at around the time of 35s. It is seen that the fluctuation is markedly increased for the argon ion laser compared with the VECSEL source.

The outcome from these measurements is that although the frequency doubled VECSEL source compares similarly in terms of average power to the argon ion laser, it significantly outperforms it in relation to lower noise, lower cost and lower maintenance. These considerations are of particular importance where the end user wishes to perform quantitative analysis on the resultant CLSM images and where source stability is necessary for reproducible results.

Conclusion

The design and implementation of a compact and reliable frequency doubled VECSEL has been described and good quality CLSM images have been obtained.
It provides an attractive, low noise, low cost alternative to an argon ion laser an offers improved CLSM imaging. Although the output power of this source is modest, it is easily capable of CLSM as demonstrated and it has the added advantages of wavelength flexibility and tuneability, lower power consumption and lower amplitude noise over existing gas based lasers.
The successful findings of this experiment have been published [5]

References

[1] Olympus Microscopy website, http://www.olympusmicro.com (accessed August 20, 2007)

[2] Umemura N., Yoshida K., and Kato K., Phase-Matching Properties of $KnbO_3$ in the Mid-Infrared, Appl. Opt. **38**, p991 (1999)

[3] Moulton P.F., Spectroscopic and laser characteristics of $Ti:Al_2O_3$, J. Opt. Soc. Am. B **3**, 125 (1986)

[4] Lyons A.B.,and. Parish C.R., Determination of lymphocyte division by flow cytometry, J. Immunol. Methods **171**, p131 (1994)

[5] Esposito E., Keatings S., Gardner K., Harris J., Riis E., and McConnell G. Confocal laser scanning microscopy using a frequency doubled vertical external cavity surface emitting laser, Rev Sci Inst, **79**, 083702, (2008)

Chapter 5 Resonant Second Harmonic Generation

Introduction

In the previous experiment only a modest level of second harmonic power was obtained. More efficient second harmonic conversion requires higher fundamental powers at the crystal. This can be achieved by either placing the nonlinear doubling crystal inside the laser cavity (intracavity doubling) or by placing it in an external cavity where the fundamental power is enhanced (resonant frequency doubling).

Intracavity doubling is based on the concept that the intensity circulating inside a laser cavity is far higher than the output of the source, so by placing the crystal inside the optical resonator, the incident fundamental power is orders of magnitude higher and therefore the efficiency of the SHG is hugely increased.

However intracavity doubling successes have been plagued by the inherent 'green problem' whereby a deleterious fluctuation in the SHG output power is observed. [1]

The green problem arises because the intracavity nonlinear crystal generates not only second-harmonic light, but also light at the sum frequencies of the laser's different longitudinal modes. This sum-frequency generation couples the competing longitudinal modes and gives rise to chaotic behaviour as the modes gain and lose oscillating strength, producing an undesirable fluctuation in output power.

In addition to the 'green problem', intracavity frequency doubling also presents a bi-directional issue in that the circulating power in the cavity passes through the crystal in both the forward and returning direction which can lead great phase-matching and cavity stability issues.

It is therefore, due to these problematic intracavity doubling issues we choose to provide higher fundamental power to the crystal by placing it in an external resonator.

The work in this chapter will investigate resonant frequency doubling with the $KnbO_3$ crystal is placed in an external enhancement cavity which enhances the 980nm VECSEL light.

Theory of Resonant Second Harmonic Generation

The basic concept behind resonator enhanced SHG is that since only a small fraction of the fundamental light is depleted in a single pass through the nonlinear crystal, the remaining light can be redirected inside a cavity configuration so that the circulating power is built up and the light interacts with the crystal many times. Successive passes of the fundamental light inside the cavity reinforce one another, so that the circulating intensity inside the resonator becomes many times higher than the incident intensity.

The resonance condition for the enhancement cavity is satisfied when the accumulated roundtrip phase associated with propagation around the cavity, φ, is an integer multiple of 2π. ($\varphi=2m\pi$).
In most instances of resonant enhancement the light incident on the enhancement cavity is single mode. However the light emitted by the VECSEL is multi longitudinal mode. To force the VECSEL into single mode operation would require the insertion of additional optics, such as an etalon, into the VECSEL cavity [1] which in our case would complicate and disrupt the simple, compact setup.
It is the intention therefore that in this work, all modes of multi mode VECSEL source will be resonant inside the external cavity. This shall be achieved by exactly matching the round-trip length of the VECSEL cavity to the round-trip length of the enhancement cavity.

The theory of resonant SHG has been analysed by Ashkin et al [2].
If we assume the resonator configuration shown in Figure 30;

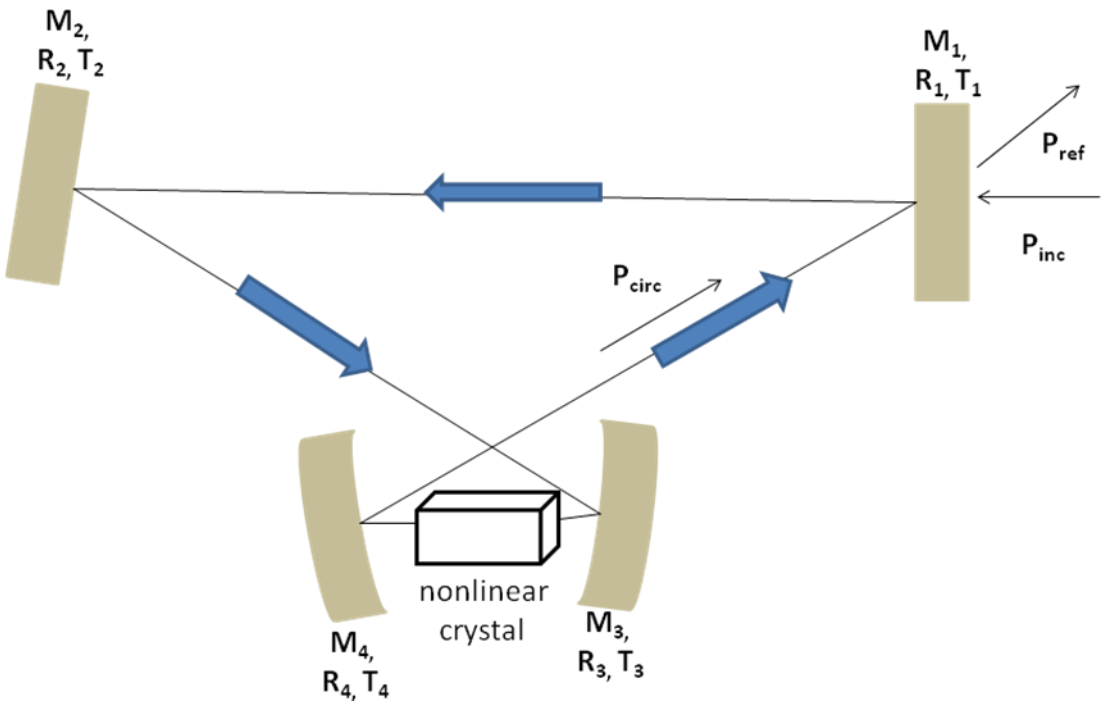

Figure 30 Cavity configuration for resonant enhancement

the ratio of circulating power, P_{circ}, to incident power, P_{inc}, on resonance ($\varphi=2m\pi$), is given by

$$\left.\frac{P_{circ}}{P_{inc}}\right|_{res} = \frac{T_1}{(1-\sqrt{R_1 R_m})^2} \qquad (11)$$

where $T_1=(1-R_1)$ is the transmission through the input coupling mirror of reflectivity R_1, and R_m represents the effective cavity reflectance

$$R_m = R_2 R_3 R_4 T T_{SHG} \qquad (12)$$

where R_i is the reflectivity of mirror M_i, T is transmission through the crystal and T_{SHG} is the loss due to SHG conversion

$$T_{SHG} = (1-\gamma_{SHG} P_{circ}) \qquad (13)$$

where γ_{SHG} is defined in Chapter 2

Off resonance, the ratio of circulating to incident power is written as

$$\frac{P_{circ}}{P_{inc}} = \frac{1-R_1}{1-2\sqrt{R_1}\sqrt{R_m}cos\phi+R_1R_m} \qquad (14)$$

The resonant second harmonic power P_{SHG}, is given by

$$P_{SHG} = \gamma_{SHG} P_{circ}^2 \qquad (15)$$

A plot $\frac{P_{circ}}{P_{inc}}$ as a function of the accumulated round trip phase, φ, for R=0.96, is shown in Figure 31.

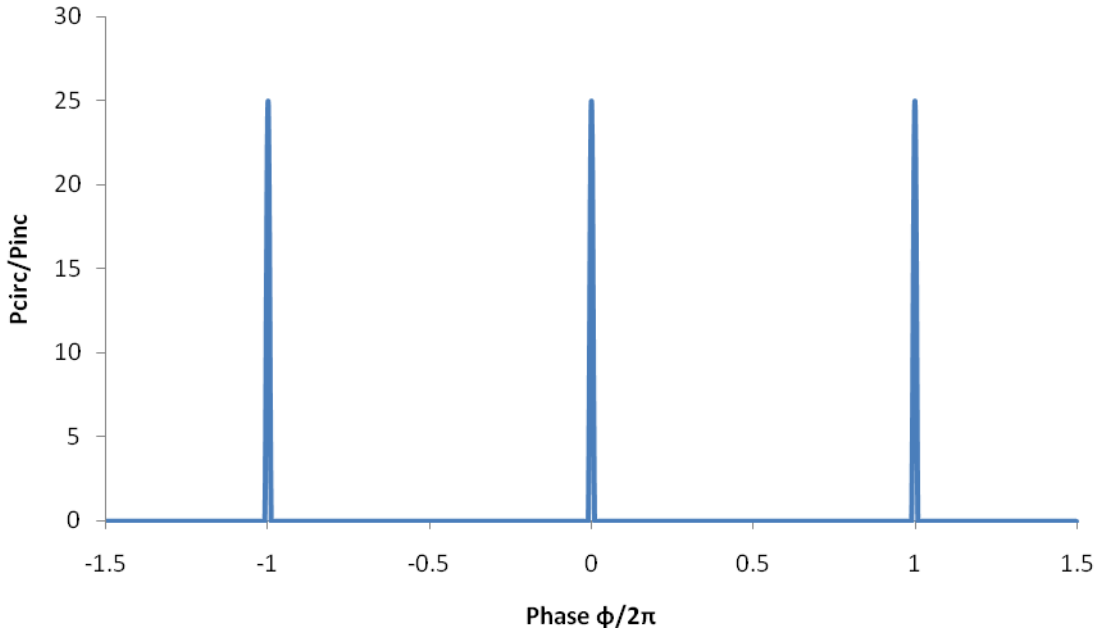

Figure 31 Enhancement cavity resonance peaks P_{circ}/P_{inc} as a function of roundtrip phase φ

This shows that at φ=2mπ there is a sharp peak in the ratio of circulating power to incident power. This corresponds to an on resonance enhancement of the light circulating inside the cavity.

Impedance-Matching

A plot of $\left.\frac{P_{circ}}{P_{inc}}\right|_{res}$ as a function of R_1 for various values of R_m is shown in Figure 32.

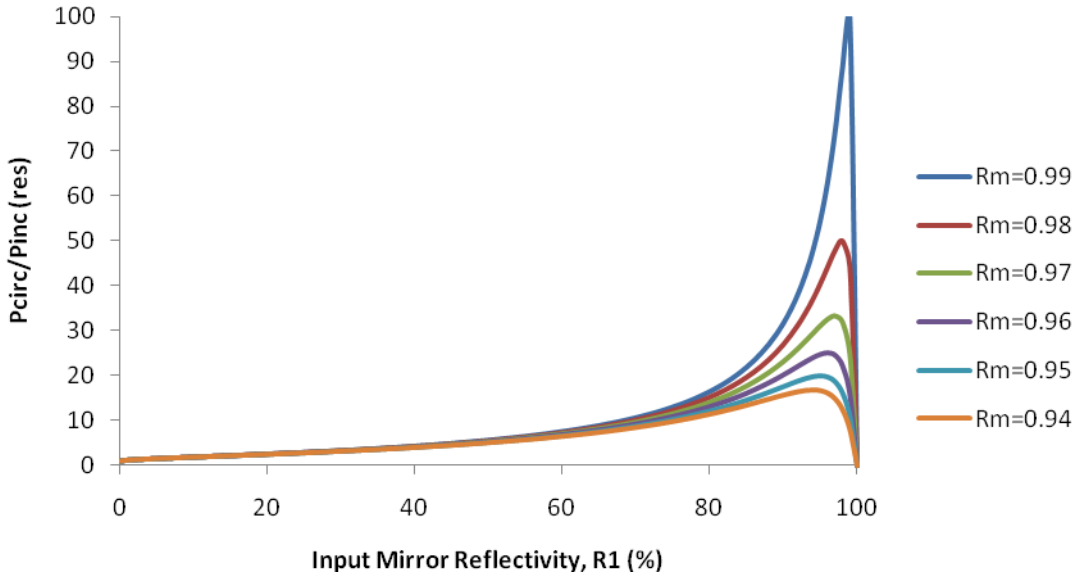

Figure 32 Ratio of circulating power to incident power as a function of input mirror reflectivity for different values of effective cavity reflectance

Two important properties of resonant cavities are evident from this figure. Firstly, the larger R_m is, the larger the power enhancement of the cavity and secondly the power enhancement is maximised when $R_1 = R_m$ (i.e the input coupling is equal to the losses inside the cavity). $R_1 = R_m$ is the condition known as impedance-matching

It is also clear from the shape of the curves in Figure 32, that if the ideal situation of perfect impedance-matching cannot be satisfied, then it is better to choose a higher input coupling value, i.e. lower reflectivity R_1, as the power enhancement falls off more gradually in this case.

If we consider the beam reflected from the resonator, it consists of two parts; the incident beam which is directly reflected from the input surface of the input coupler,

R_1, and the portion of the circulating beam which is leaked through r_1. On resonance the ratio of reflected power, P_{ref}, to incident power, P_{inc}, can be written as

$$\left.\frac{P_{ref}}{Pinc}\right|_{res} = \left(\frac{\sqrt{R_1}-\sqrt{R_m}}{1-\sqrt{R_1 R_m}}\right)^2 \qquad (16)$$

A plot of $\left.\frac{P_{ref}}{P_{inc}}\right|_{res}$ as a function of input mirror reflectivity, for R_m=0.96, is shown in Figure 33.

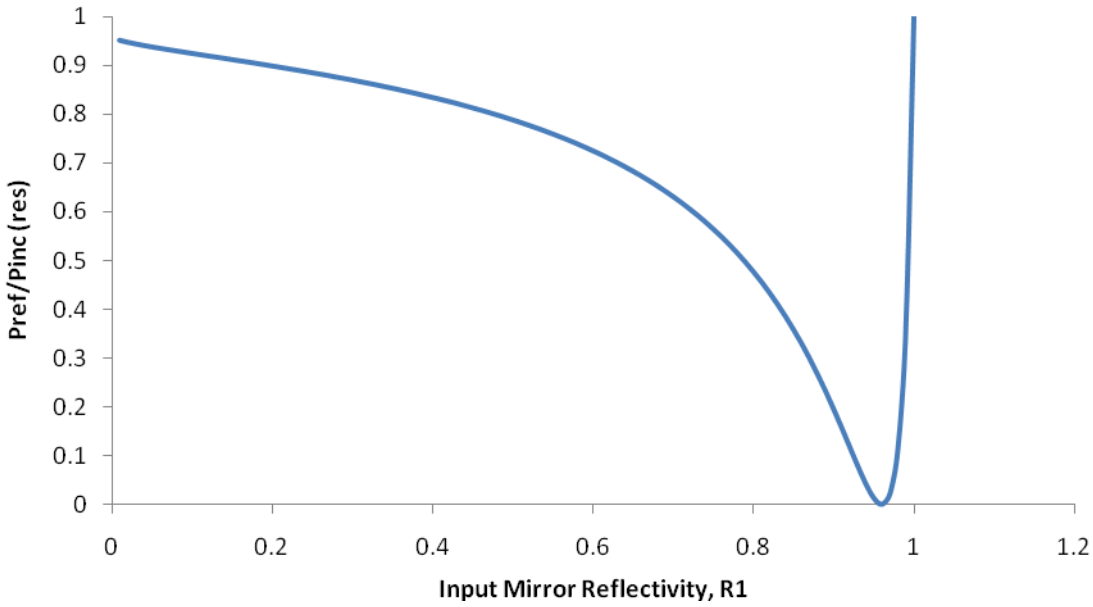

Figure 33 Ratio of reflected power to incident power

From this figure, we can see that when the impedance-matching condition is met, the amplitude of the ratio of reflected to incident power is zero, indicating that all the power incident on the resonator is coupled into it.

Also from this figure, we can see that it is still possible to couple a high percentage of the light into the cavity (>50%) even if the impedance matching condition is not

met but the input mirror reflectivity R_1 is lower than the effective cavity reflectance R_m.

In this experiment, the input coupling value was chosen to be 4% (R_1=0.96) for expected optimum impedance matching, which would result in a enhancement of 25 times more circulating power to incident power. For 400mW of VECSEL incident power this corresponds to an expected circulating power of 10W from which, taking into account pump depletion as discussed in Chapter 2, it is reasonable to expect approximately 200mW of resonant second harmonic blue power to be generated.

Hansch-Couillaud Frequency Locking

To provide a constant second harmonic power generated from the enhancement cavity, the cavity length must be stabilised (i.e locked in frequency) to ensure that it is always resonant with the fundamental beam.

A variety of techniques to counteract the effects of temperature changes and mechanical vibrations, which can cause a drift in the cavity length, have been applied to enhancement cavities [3,4]. Generally, an electrical error signal is generated which has a magnitude proportional to the deviation between the laser frequency and the cavity resonant frequency, and a sign that indicates whether the laser frequency is above or below the resonant frequency.

The electronic, frequency locking technique applied in this experiment is Hansch-Couillaud locking [4]. This method utilises the presence of the nonlinear crystal within the external resonator as an intracavity polarizer, and monitors changes in the polarization of the light reflected by the resonator to generate an error signal with a magnitude proportional to the deviation between the VECSEL laser frequency and the resonant frequency of the enhancement cavity.

The application of this technique to our experimental setup is illustrated in Figure 34.

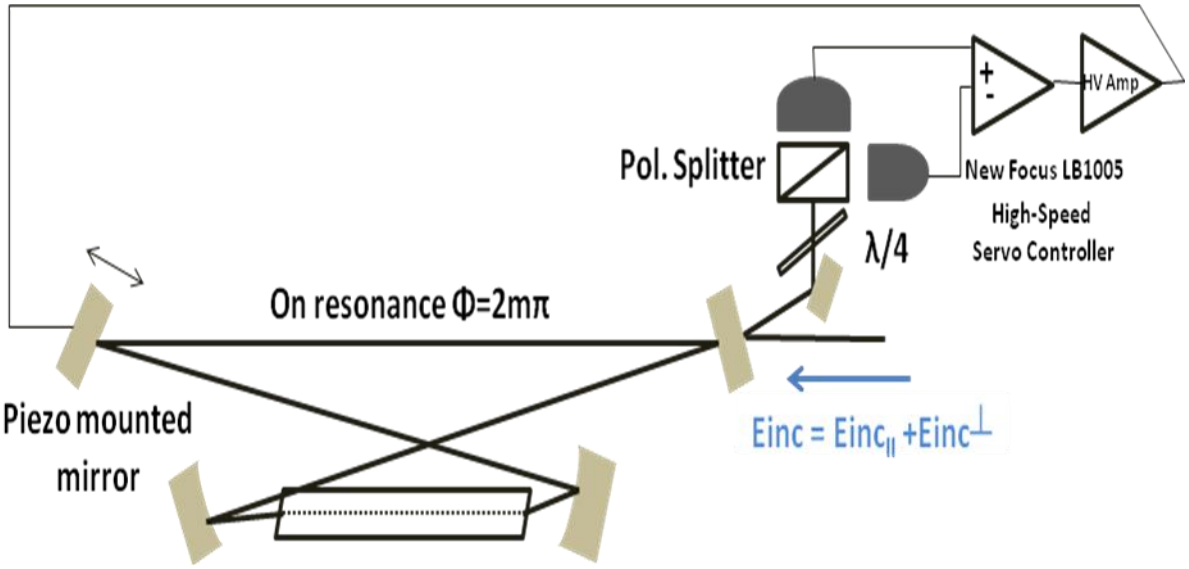

Figure 34 **Hansch-Couillaud Locking Setup**

The light emitted from the VECSEL cavity is in a linear polarization state at some angle with respect to the plane of the external ring cavity, which can be decomposed into two orthogonal components, $E_{inc\parallel}$ parallel to the plane of the ring and $E_{inc\perp}$, perpendicular to the plane of the ring.

Due to the presence of the birefringent crystal within the resonator, only the perpendicular component resonates around the ring. The light reflected by the resonator can therefore be decomposed into the following two components;

$$\tilde{E}_{ref_{\parallel}} = r_1 \tilde{E}_{inc_{\parallel}} \qquad (17)$$

and

$$\tilde{E}_{ref_{\perp}} = r_1 \tilde{E}_{inc_{\perp}} + it_1 r_m e^{i\phi} \tilde{E}_{circ_{\perp}} = \left(\frac{r_1 - r_m e^{i\phi}}{1 - r_1 r_m e^{i\phi}} \right) \tilde{E}_{inc_{\perp}} \qquad (18)$$

where $r = \sqrt{R}$. At exact resonance ($\phi = 2m\pi$), the reflected beam components remain in phase and the beam is linearly polarized. Away from resonance the perpendicular component acquires a phase shift, $\Delta\phi$, relative to the parallel component resulting in an elliptically polarised reflected beam where the 'handedness of the ellipticity depends on the sign of the detuning from resonance as shown in Figure 35 (a).

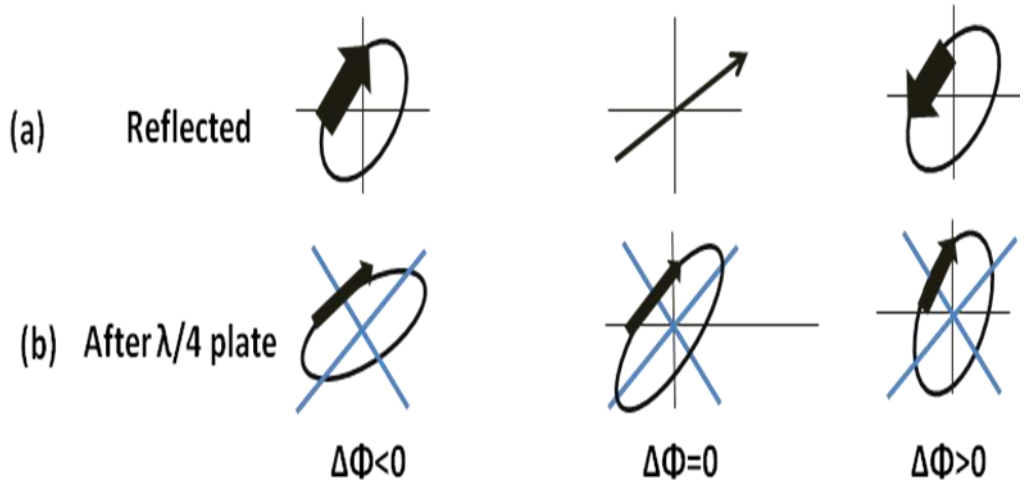

Figure 35 Polarisation states involved in generating the error signal for Hansch Couillaud locking (a) reflected from resonator (b) after λ/4 waveplate [5]

The reflected beam is then passed through the λ/4 retarder followed by a polarizing beamsplitter with the fast and slow axes of the retarder aligned at 45 degrees to the axes of the beamsplitter. The light intensities of the separated components are monitored by two photodiode detectors. The λ/4 retarder transforms the elliptically polarized beam into orthogonal linearly polarised waves which are separated by the beamsplitter so that the intensities can be measured by the photodiodes. Off resonance, when the VECSEL frequency is above the resonant frequency of the external cavity, one of the measured intensities will exceed the other by an amount proportional to the magnitude of the frequency detuning and the relationship is reversed when the VECSEL frequency is below resonance. On resonance, the linearly polarized beam will be separated into two components of equal intensity. The signals from the two detectors (OSRAM Opto Semiconductors PIN photodiodes BPW 34B) are subtracted, using the circuitry, shown in Figure 36, and the resulting error signal was then input into a New Focus LB1005 High-Speed Servo Controller integrator unit. The gain of an integrator drops by 6 dB/octave. The time constant of the integrator (the inverse of the frequency, where the gain has dropped to 0

dB) is used to control the gain of the feedback loop. As the time constant is decreased (gain increased) and the servo loop starts responding at higher frequencies one typically sees the lock tightening through a reduction in the error signal detected by the photodiodes. Associated with the integrator is also a 90 degree phase shift. As this is added to the other phase shifts in the feedback loop (HV amplifier and piezo) there will eventually be a frequency, at which the gain exceeds unity and the feedback is positive. At this point the circuitsstarts oscillating violently. For normal stable operation the gain is chosen slightly below this point. The signal from the integrator is sent to the HV Amp which drives the piezo mirror within the cavity, adjusting the cavity length so that it always remained on resonance.

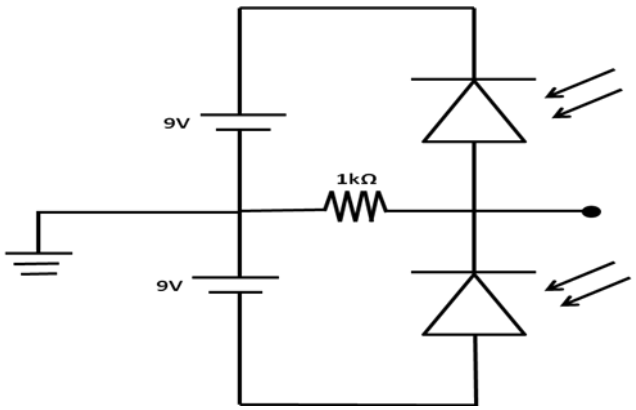

Figure 36 Subtraction circuit

Experiment

The enhancement cavity setup, shown in Figure 37, was designed, using WinLase software, with the mirror radius of curvature and the separations chosen to ensure a stable cavity. The roundtrip length for this cavity was 899mm

The length of folding arm inside the VECSEL cavity (shown in Chapter 3) was changed to 339mm in order to exactly match the roundtrip lengths of both cavities.

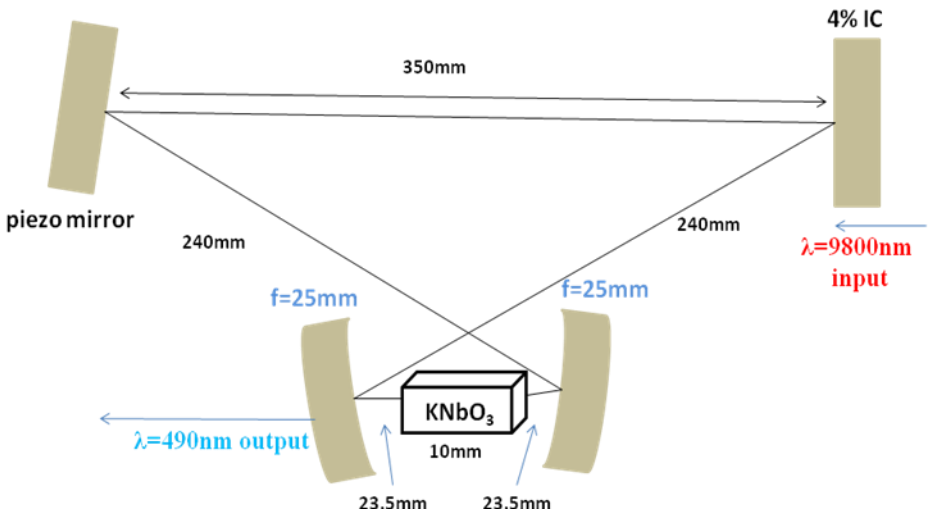

Figure 37 Enhancement Cavity Setup

There were two main advantages of using a ring cavity instead of a linear cavity. Firstly, in this configuration the pump laser (VECSEL) receives minimal feedback from light circulating around the enhancement cavity which ensures stable operation. Secondly, as this cavity geometry only allows for propagation of the fundamental beam around the cavity in one direction, the second harmonic is also only emitted in one direction, thus ensuring a more efficient and useful process.

We have seen already in Chapter 2 that SHG of gaussian beams is maximised by optimium Boyd-Kleinmann focusing of the fundamental beam into the nonlinear crystal. Thus, it was also an important consideration in the design of the resonator that the beam it confines is focused to, the previously calculated, ω_0=16μm inside the nonlinear crystal.

Figure 38 shows that this cavity design does indeed provide the optimum focusing of the circulating beam exactly halfway along the length of the nonlinear crystal.

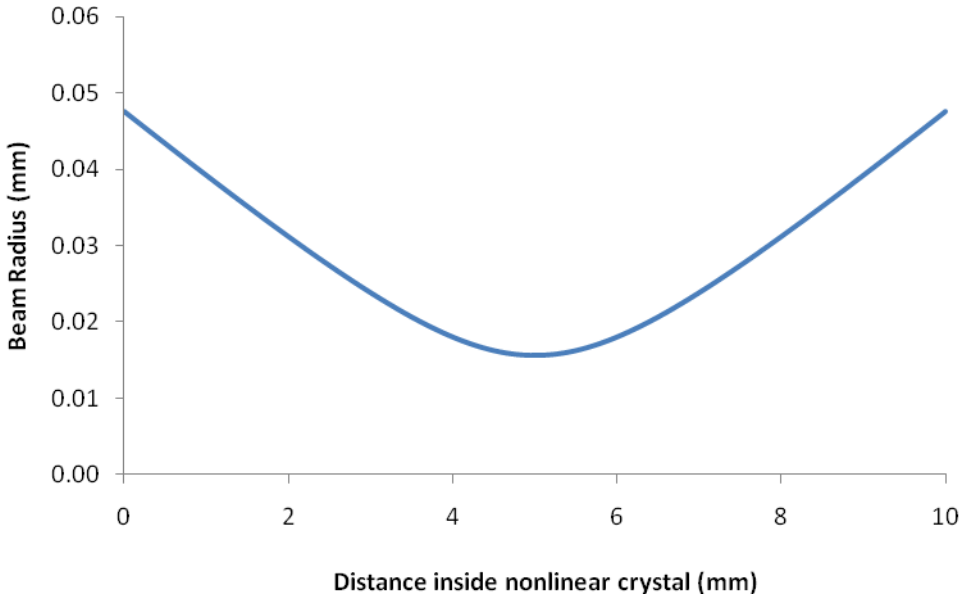

Figure 38 Focusing inside the nonlinear crystal

The VECSEL beam was focused into the external ring cavity to provide optimum focusing into the crystal using a series of mode-matching lenses.

The mode –matching lens configuration was designed to take the beam of radius 361μm emerging from the VECSEL cavity and focus it to a radius of ~320μm halfway along the length of the first arm inside the external cavity, as required by its geometry in order to achieve optimum Boyd-Kleinmann focusing inside the nonlinear crystal. The external cavity geometry then acts to focus the circulating beam to the required 16μm radius inside the nonlinear crystal.

The entire experimental setup is shown in Figure 39.

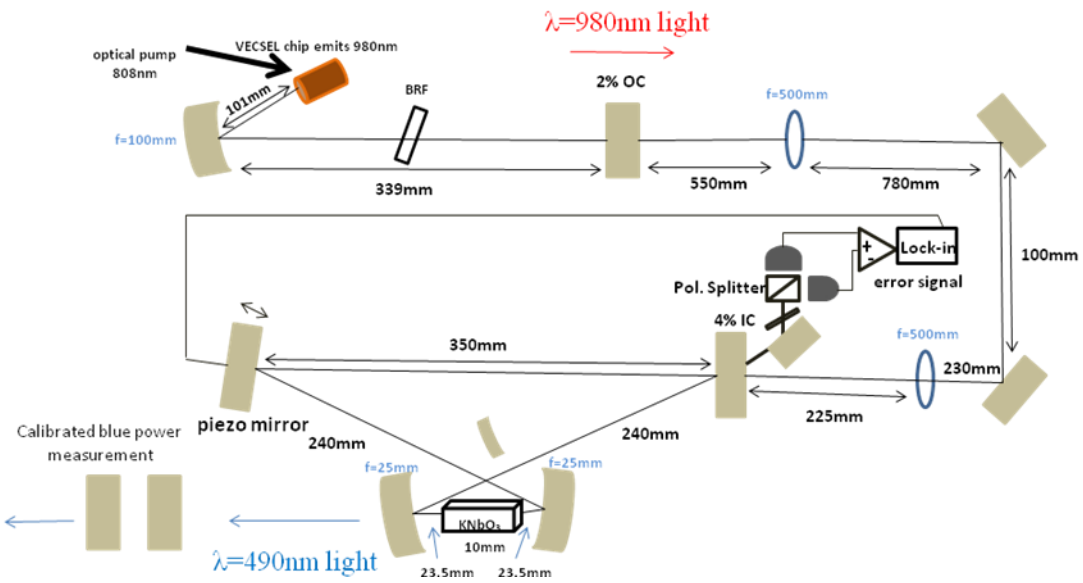

Figure 39 Overall Experimental Setup

Figure 40 shows the propagation of the beam throughout the entire configuration.

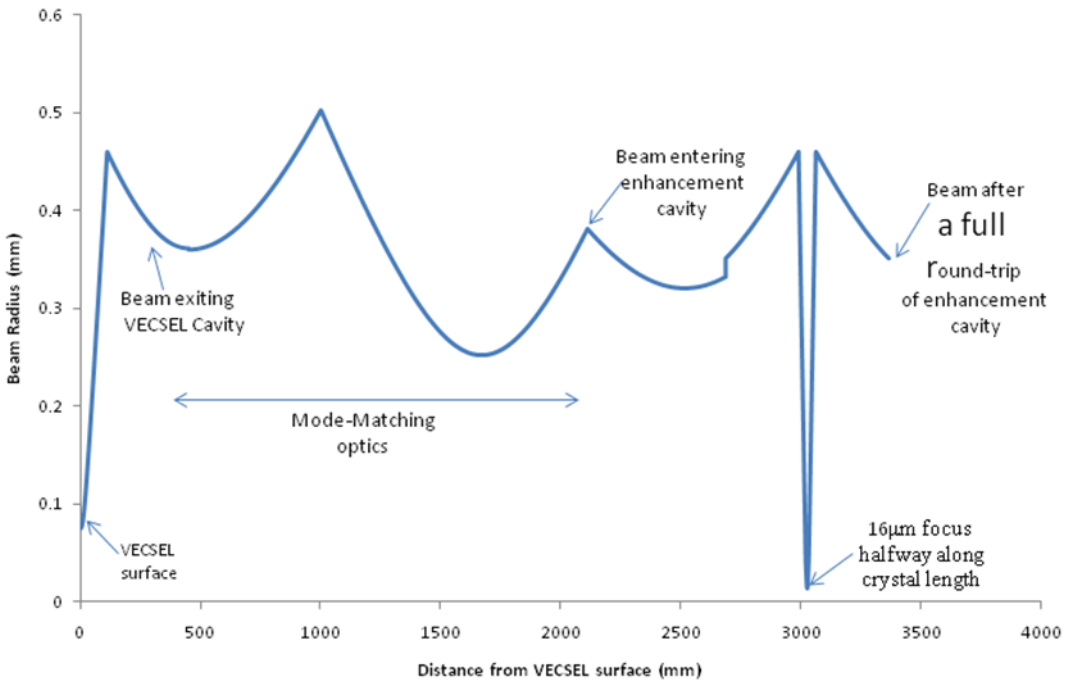

Figure 40 Beam radius propagation throughout entire configuration

Cavity Alignment

Firstly, the enhancement cavity was set up without the input coupler and mirror M4, in a single pass configuration for optimisation of the mode matching and focusing into the crystal. The leakage of the single pass beam from mirror M3 was calibrated using a photodiode detector so that this could be compared with that for the completed cavity in order for a measurement of the circulating power in the cavity to be taken.

With the insertion of mirror M4 and the input coupler the ring cavity was completed and the piezo mirror was set to scan the cavity length through one free spectral range and a cavity resonance via a voltage ramp driven by a signal generator.

At this stage, an etalon was inserted inside the VECSEL cavity. This brings the laser into single frequency operation which was monitored using a scanning Fabry Perot interferometer. The insertion of the etalon means that there is only one longitudinal

mode available to circulate inside the enhancement cavity and therefore it easier to align.

To monitor the alignment of the cavity, a photodiode detector was placed at mirror M4, and its response through each piezo sweep is viewed on a standard oscilloscope.

Figure 41 shows the alignment of the ring cavity with the VECSEL operating in single mode

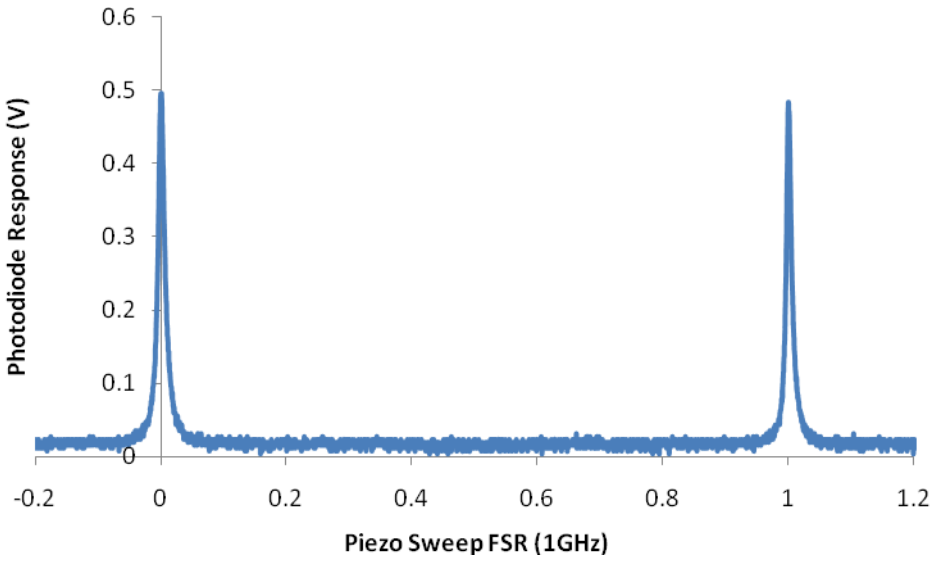

Figure 41 Single Frequency Ring Cavity Alignment

This indicates that the ring cavity contains no circulating higher-order modes and resonant enhancement of the single mode is observed.

With the ring cavity well aligned for the VECSEL operating in a single frequency, the etalon was removed from the VECSEL cavity. This brought the laser back into multimode operation, and it was observed that the circulating longitudinal modes were resonant at different cavity lengths.

By finely tuning the VECSEL cavity length, using the output coupler mirror micrometer adjustment, a gradual shift towards resonance of the longitudinal modes was observed until the situation where complete resonant enhancement of the multi

mode VECSEL light occurred. At this point the VECSEL roundtrip length is exactly matched to the enhancement cavity roundtrip and all the circulating modes are resonant inside the cavity.

The shift towards multi-mode resonance is shown in Figure 42.

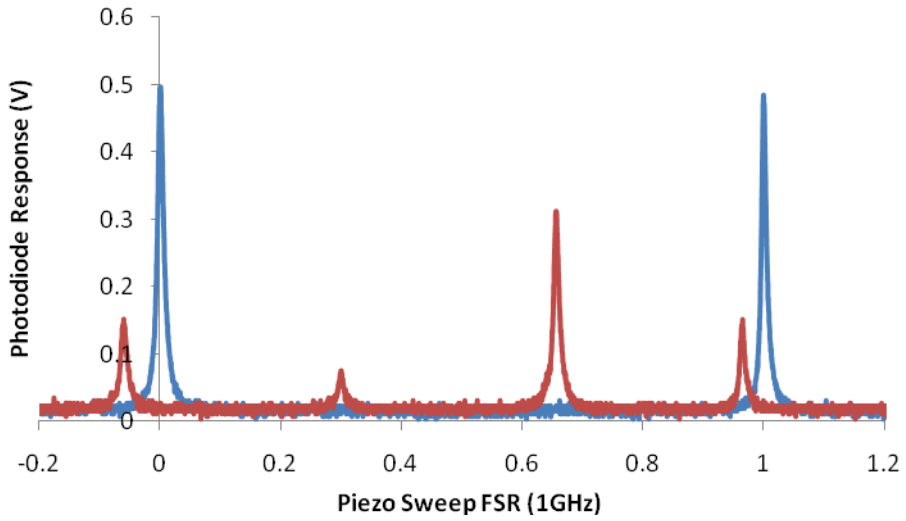

Figure 42 Longitudinal modes circulating inside cavity off and on resonance

To ensure that the cavity was fully aligned for the VECSEL operating in multi longitudinal mode, the resonance peaks were observed for single mode, few mode, and multi mode operation of the VECSEL. As can be seen in the following Figures, the resonance peaks observed remain unchanged for each mode situation, indicating that the enhancement cavity was fully aligned with all modes resonating inside the cavity.

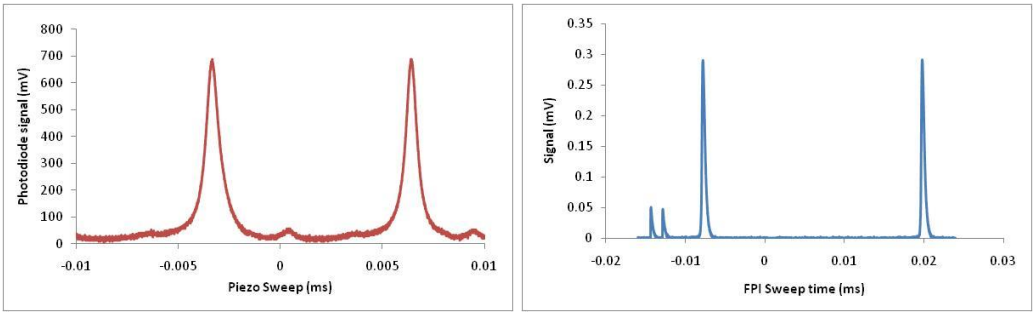

Figure 43 **(a) Resonance peaks observed for the ring cavity with the VECSEL operating in single mode operation, as shown in (b)**

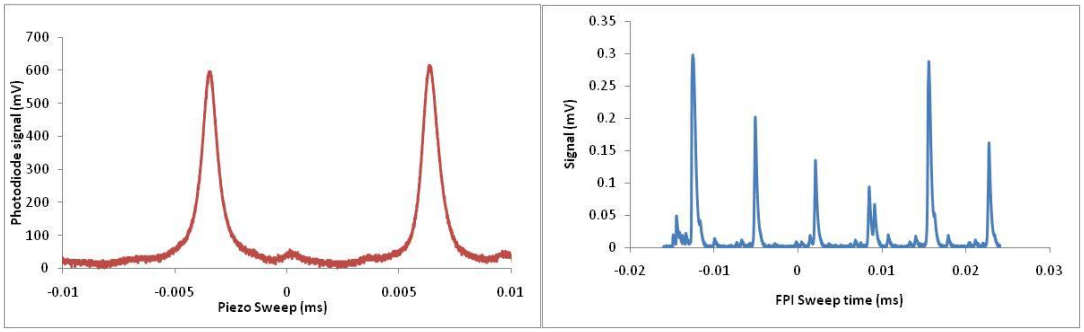

Figure 44 **(a) Resonance peaks for the ring cavity observed with the VECSEL operating in few mode operation as shown in (b)**

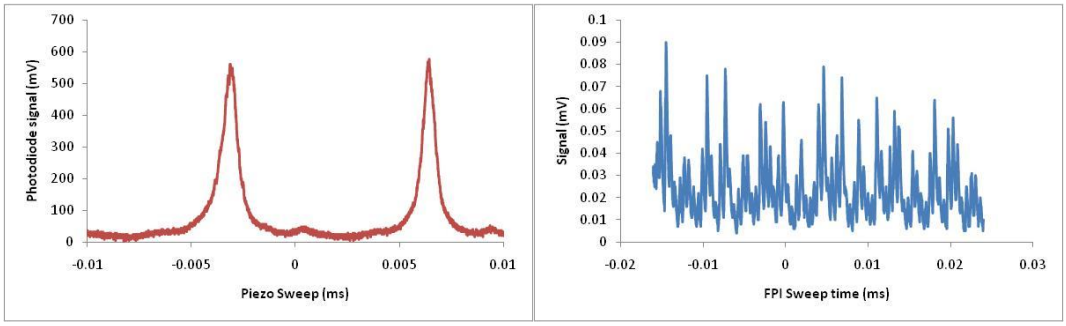

Figure 45 **(a) Resonance peaks observed for the ring cavity with the VECSEL in multi mode operation as shown in (b)**

The figures above also illustrate a broadening of the resonance peaks with the VECSEL operating in multimode in comparison to the single mode resonance peaks observed in Figure 41. This indicates that a lower cavity finesse value is expected in the case of multimode operation.

With the ring cavity critically aligned and the VECSEL operating in multimode, the crystal was cooled from room temperature to the previously determined 10º C required for SHG phase matching.

Characterisation of the Source

Circulating Power

By measuring the IR leakage from mirror M3, the ratio of circulating power to incident power was determined to be 7. For an incident power of 400mW this corresponds to a circulating power of 2.8W

Impedance Matching

Figure 46 shows the normalized signal detected by a photodetector monitoring the light reflected from M1 as the cavity length is scanned by one free spectral range by the sweeping piezo.

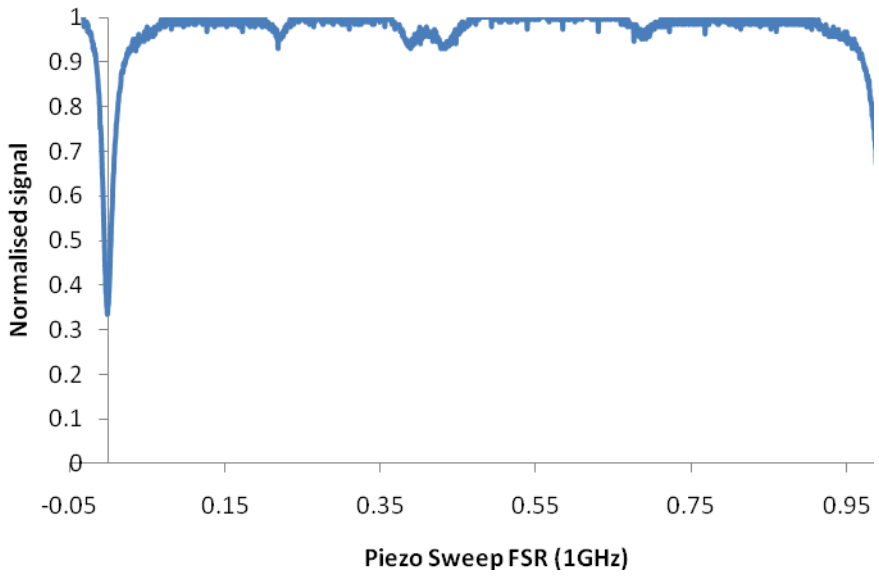

Figure 46 Normalised light reflected by the cavity

This figure indicates that on resonance; approximately 70% of the incident light is coupled into the cavity. As previously discussed, perfect impedance matching is when 100% is coupled into the cavity.

Cavity Finesse

The enhancement cavity finesse was determined by measuring the free spectral range (i.e the separation of the peaks) divided by the full width at half maximum of the resonances (i.e their width) as illustrated in Figure 47.

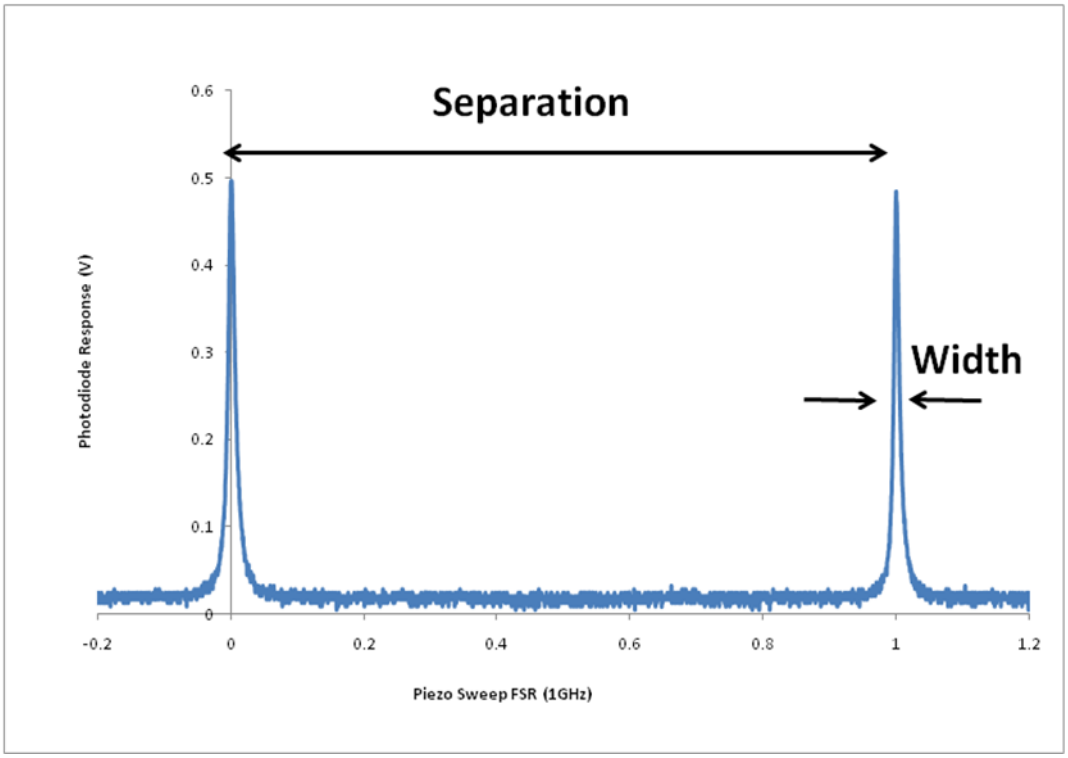

Figure 47 Cavity Finesse measurement

The finesse of the fully aligned resonant SHG cavity was measured as >100 with the VECSEL operating as single frequency however this was reduced to 50 for multi mode operation of the VECSEL. This was attributed to higher dispersion in the multi mode cavity.

Resonant Second Harmonic Power

With the cavity stabilised in length by the Hansch Couillaud frequency locking system, 4.5mW of resonant second harmonic power at 490nm was generated for 400mW of power incident on the cavity at 980nm.

Discussion

As can be seen from these results the generated second harmonic power and the ratio of circulating power to incident power are much lower than the expected values for this enhancement cavity design.

A plot of $\left.\frac{P_{circ}}{P_{inc}}\right|_{res}$ against effective cavity reflectance R_m, as shown in Figure 48, shows that on resonance, an enhancement factor of 7 corresponds to an effective cavity reflectance of 0.89.

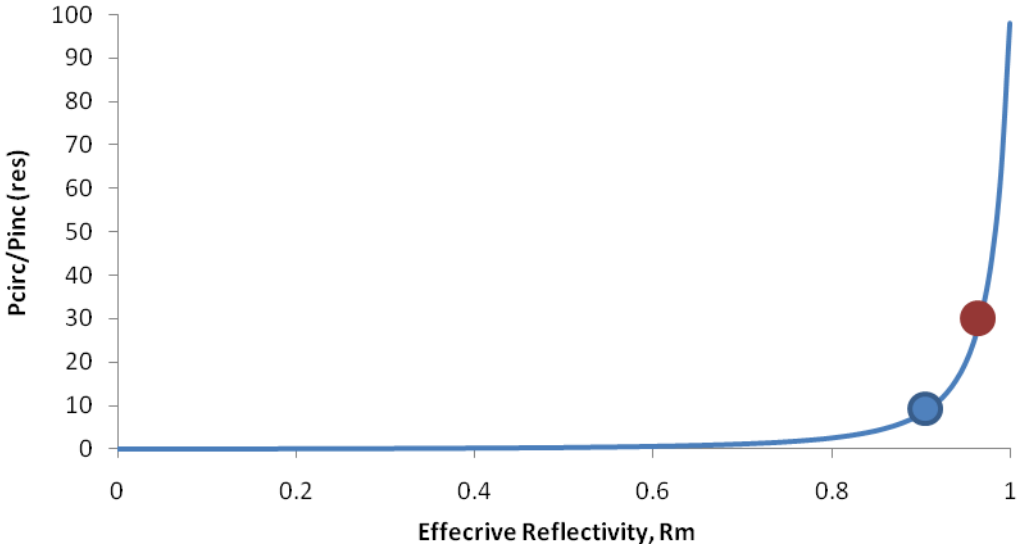

Figure 48 **P_{circ}/P_{inc} (res) against effective reflectivity, r_m. The red circle indicates the theoretically expected value and the blue circle indicates the experimentally measured value**

This means that the enhancement cavity experiences a loss of 11% for each roundtrip.

This is confirmed in a plot of $\left.\frac{P_{ref}}{P_{inc}}\right|_{res}$ against R_m, as shown in Figure 49 ,which shows that for the 70% impedance matching that was measured experimentally the effective cavity reflectance is 0.89.

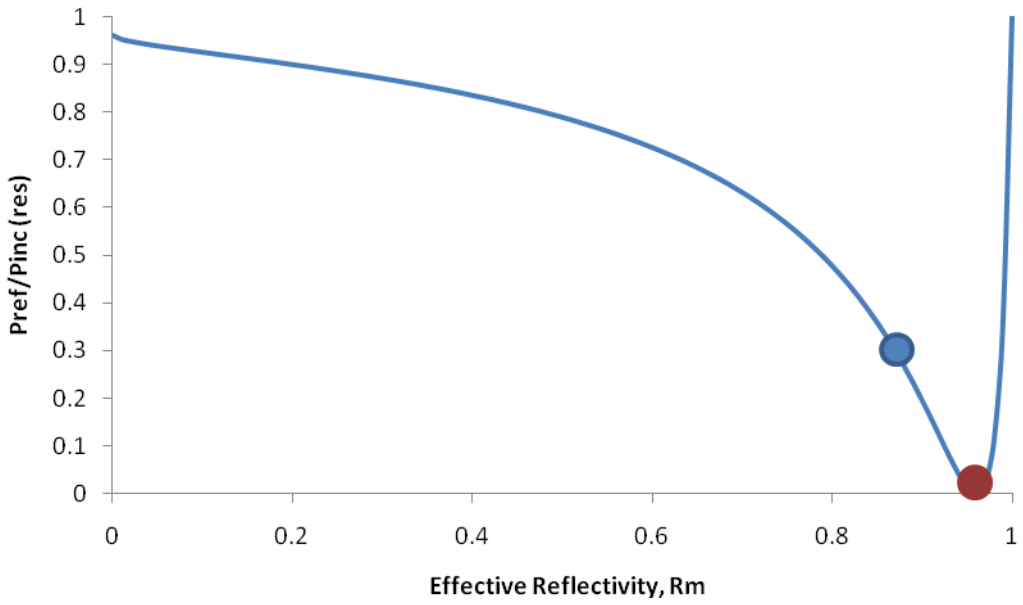

Figure 49 **P_{ref}/P_{inc} (res) against effective reflectivity, r_m. The red circle indicates the theoretically expected value and the blue circle indicates the experimentally measured value**

An 11% loss inside the enhancement cavity far exceeds the estimated 4% roundtrip loss. An investigation reveals that the source of this loss is the crystal transmission at 980nm. A measurement of the power before and after exiting the crystal, at a temperature far from the phase matching temperature of 8 degrees , shows that there is an overall loss of 8% in transmission through the crystal indicating an 4% loss at each surface of the crystal. A reasonable explanation for this, is, that the anti-reflection coating applied to the crystal has degraded in the time period between this experiment and the single pass SHG experiment.

The 8% crystal transmission loss along with a further 3% for all other losses in the cavity (including SHG conversion and transmission through the mirrors) accounts for the 11% overall loss measured in the system.

This large unexpected cavity loss prevents the impedance matching condition from being satisfied and explains the low second harmonic power that is generated.

A summary of the expected results against the experimentally measured values for the cavity are shown in Table 2.

	Expected value	**Measured value**
$\mathbf{P_{inc}}$	400mW	400mW
$\mathbf{P_{circ}}$	10W	2.8W
$\mathbf{P_{circ}/P_{inc}}$ **(res)**	25	7
$\mathbf{P_{ref}/P_{inc}}$ **(res)**	0	0.3
$\mathbf{R_m}$	$=R_1=0.96$	0.89
$\mathbf{P_{SHG}}$	~200mW	4.5mW

Table 2 Summary of theoretically expected results and experimentally obtained values

Conclusion

This chapter describes the resonant second harmonic generation of the VECSEL source with the $KNbO_3$ crystal placed in an external ring cavity designed to enhance the 980nm VECSEL light. The cavity design and implementation along with important theoretical considerations are presented. Unfortunately throughout the course of the experiment the crystal ceased to function as expected and so high unexpected cavity losses and low resonant SHG power were observed. However the observations of a well aligned frequency locked doubling enhancement cavity indicate that the experiment has the potential for success if the crystal problems are resolved.

References

[1] Gardner K.S., Abram R.H., Riis E., A birefringent etalon as a single mode selector in a laser cavity, Optics Express, **12**, 12, 2004

[2] Ashkin A., Boyd G.D., Dziedzic J.M., Resonant optical second harmonic generation and mixing, IEEE Jour Quant Elec, **2,** 1966, 109

[3] Drever R.W.P., Hall J.L., Kowalski F.V., Hough J., Ford G.M., Munley A.J., Ward H., Laser phase and frequency stabilization using an optical resonator, Appl Phys B, **31**, 1983, 97

[4] Hansch T.W., Couillaud B., Laser frequency stabilization by polarization specroscopy of a reflecting reference cavity, Opt. Commun. **35**, 441 (1980)

[5] Compact Blue-Green Lasers, Risk, Gosnell & Nurmikko, published by Cambridge University Press, 2003

Chapter 6 Sum Frequency Generation

Introduction

As previously discussed, schemes to produce blue light by SFG, often mix a very strong pump beam at wavelength λ_2, with a much weaker probe at λ_1 by which it is possible for complete conversion of the probe into a visible beam at wavelength λ_3.

In this chapter we present the theoretical considerations and the experimental planning for sum frequency generation between our resonantly enhanced 980nm VECSEL as a weak probe and a strong diode pumped mode locked 1047nm NdYLF laser in $KNbO_3$ to give short, high power blue pulses at 504nm. A similar experimental process has been investigated by Albota and Wong [1] whereby they have utilised the concept of unity conversion for single photon detection using Si avalanche photodiode single photon counting modules.

Experimental Design.

The high power pump source would be a Microlase Optical systems DPM 1000 diode pumped mode locked NdYLF laser providing 3ps pulses at a repetition rate of 120MHz with a peak pulse energy of 12nJ at 1047nm.

The weaker probe signal would be provided by the resonant enhancement of the 980nm VECSEL as described in Chapter 5 and in fulfilling its aim this experiment would demonstrate a complete conversion of the incident power of this source to SFG blue light at 504nm.

The proposed experimental setup is shown in Figure 50

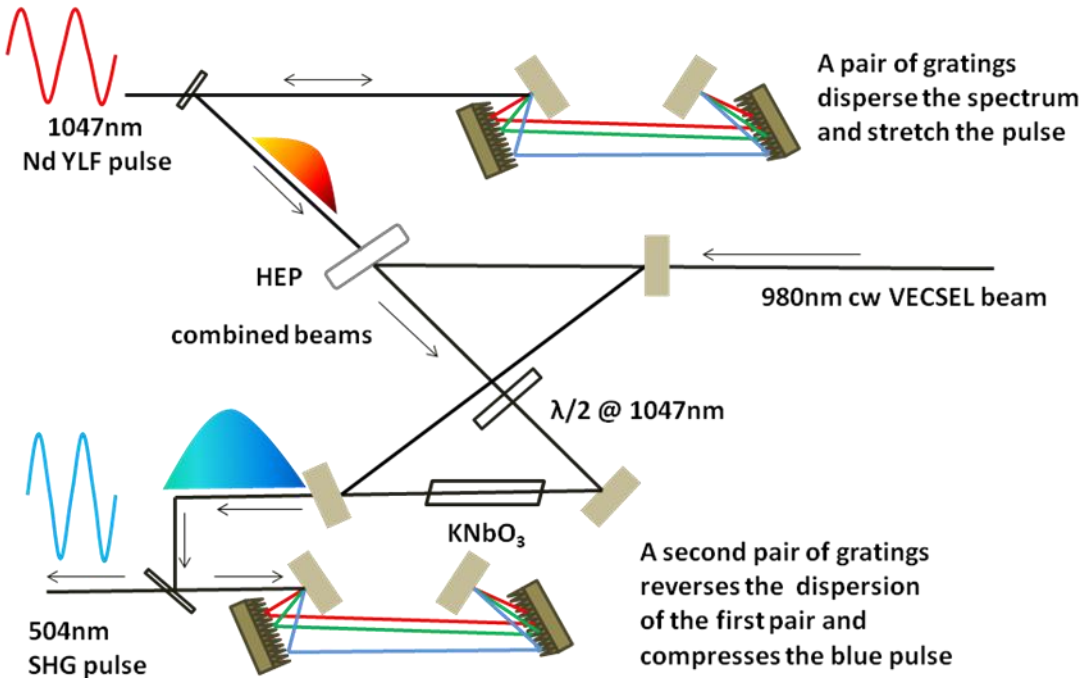

Figure 50 Proposed SFG Experiment

The cavity is single pass for the 1047nm pump through the crystal and the 980nm VECSEL probe is resonated in the same ring configuration described in the previous chapter. The pump source would be coupled into the ring cavity using a Newport high energy polariser (HEP) which reflects s-polarised light at the pump wavelength and transmits p-polarised probe light, and with appropriate mode matching optics the pump and probe beam will be optimally focused for interaction together inside the nonlinear crystal.

A λ/2 waveplate designed for 1047nm will also inserted into the cavity to ensure that the correct polarisation is incident on the crystal.

Phase matching for SFG at these wavelengths occurs at a temperature of ~ 83degrees calculated using the Sellmier equations for $KNbO_3$ [2]. Control of the crystal temperature would be achieved by housing it in a homemade copper oven.

The peak power supplied in each pulse from the pump source is ~4000W. Calculation, using the equations described in Chapter 2, determines that 62W is the pump power required to achieve unity conversion efficiency of the probe. As the

power that the pump source provides far exceeds the required 62W, the experimental setup will involve firstly sending the pump beam through a pair of gratings in order to stretch the pulse. Stretching the pulse will reduce the peak pulse power by the required amount and it will also increase its duration. This will benefit the SFG process as the longer the pulse and the cw VECSEL beam interact inside the crystal the higher conversion efficiency.

The output SFG pulse at 504nm exiting the cavity would then be directed into another grating pair where it would then be compressed. The outcome of this would be short high power pulses in the visible region.

Conclusion

In this chapter, the theoretical considerations and the experimental planning for sum frequency generation between our resonantly enhanced 980nm VECSEL and a strong diode pumped mode locked 1047nm NdYLF laser in $KNbO_3$ are presented. The aim of this experiment would be to achieve unity conversion efficiency of the VECSEL probe power into an output of short, high power pulses in the desirable blue wavelength region. This experiment would have potential for various imaging applications.

References

[1] Albota M.A., Wong F.N.C., Efficient single-photon counting at 1.55μm by means of frequency upconversion, Optics Letters, **29**, 13, 2004, 1449

[2] Umemura N., Yoshida K., and Kato K., Phase-Matching Properties of $KNbO_3$ in the Mid-Infrared, Appl. Opt. **38**, p991 (1999)

Overall Conclusion

A brief introduction to the applications and basic configuration of vertical external cavity surface emitting lasers is given in Chapter 1.

Chapter 2 introduces the basic principles of nonlinear optics and describes in detail two nonlinear processes which are the focus of this work; second harmonic generation and sum frequency generation. The important conditions for optimised frequency conversion are also discussed.

In this work a homemade optically pumped VECSEL emitting at 980nm was constructed. The optical pump profile analysis and the characterisation of this source are presented in Chapter 3.

Second harmonic generation of the VECSEL through a single pass of the nonlinear crystal $KNbO_3$ is demonstrated and successful CLSM images are obtained using this source as described in Chapter 4.
This work in this chapter highlights the scope for frequency doubled VECSELs in applications of biophotonics and the findings have been published.

In an attempt to increase the nonlinear frequency conversion efficiency achieved in the previous chapter, SHG by resonant enhancement of the fundamental VECSEL light in an external cavity is presented in Chapter 5. The important theoretical considerations involved in resonant SHG are described in detail and our experimental findings are presented. Unfortunately throughout the course of this experiment the nonlinear crystal ceased to function as expected and the impact of this is also discussed.

In the final chapter the experimental planning for sum frequency generation between our resonantly enhanced 980nm VECSEL and a diode pumped mode locked 1047nm NdYLF laser in $KNbO_3$ to give short, high power blue pulses at 504nm is presented.